Published OnlineFirst August 18, 2010; DOI:10.1158/1078-0432.CCR-09-2660



when analyzed in a model with *MYCN*, stage, and age in a logistic regression analysis (data not shown).

### *ALK* low copy number gain, gene expression, and survival

Low copy number gain of chromosome 2p material or whole chromosome 2 gain was detected in 19.3% (49 of

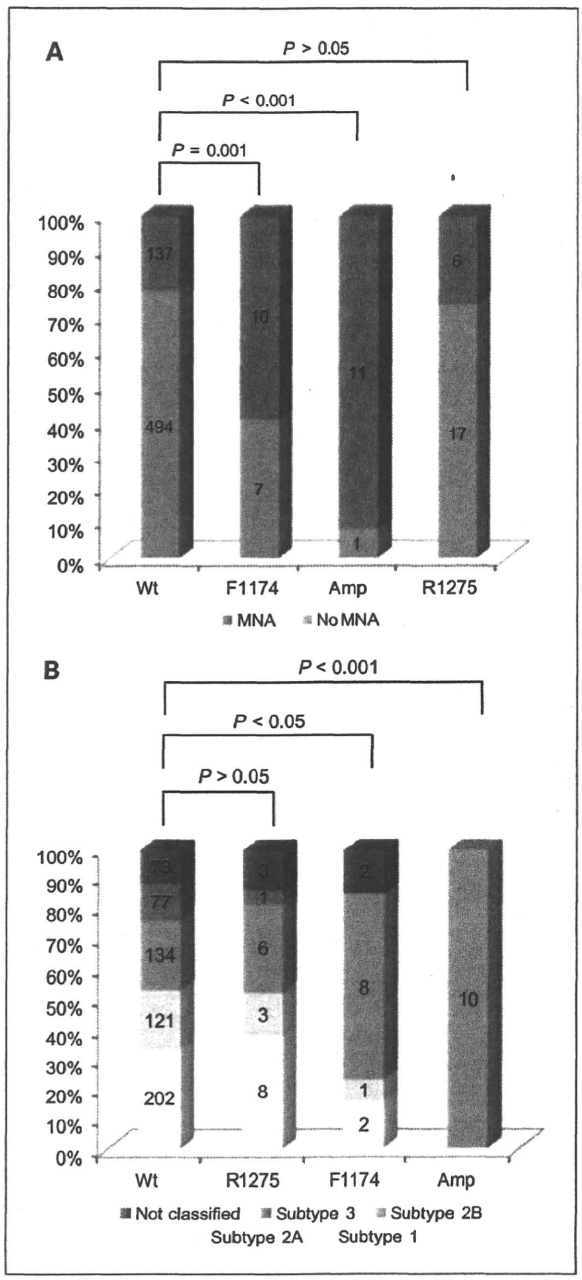


Fig. 1. Comparison of the distribution of *MYCN* status (A) and genomic subtype (B) in tumors with one of the two frequent *ALK* mutations or *ALK* amplification versus wild-type tumors. Wt, wild-type *ALK*; Amp, *ALK* amplification; MNA, *MYCN* amplification.

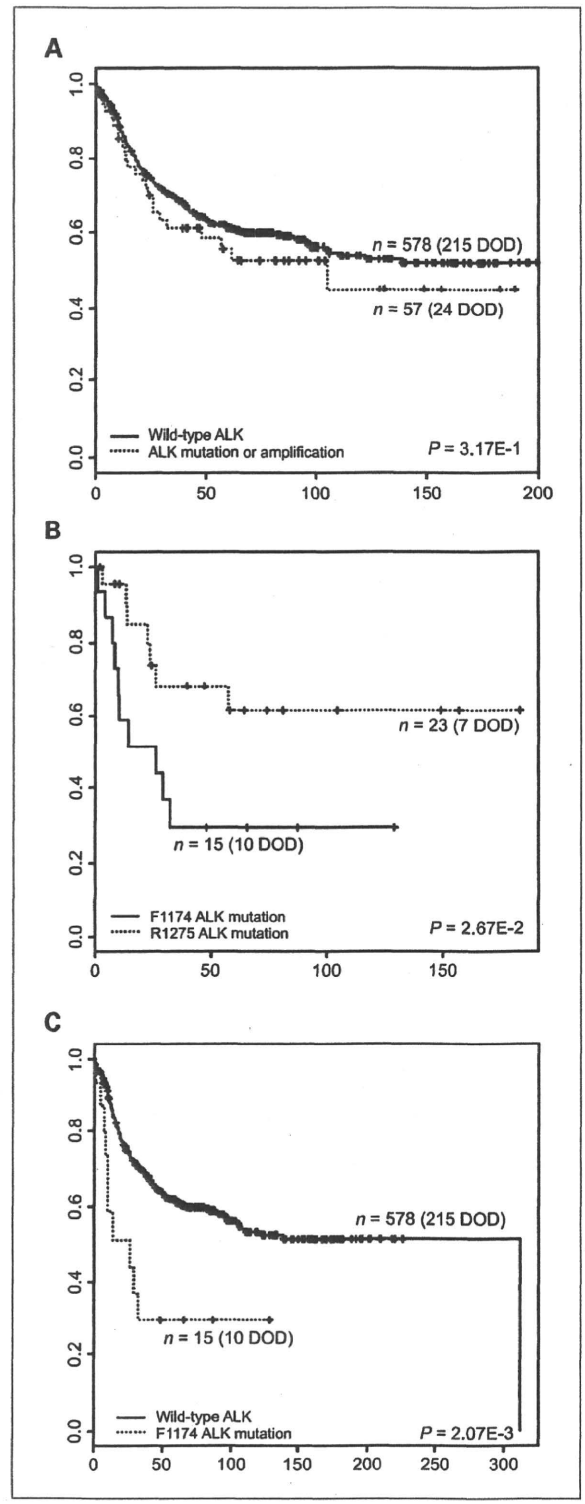


Fig. 2. Kaplan-Meier and log-rank analysis of *ALK*-mutated and *ALK*-amplified tumors versus *ALK* wild-type cases (A), F1174 mutated versus R1275 mutated cases (B), and F1174 mutated versus wild-type cases (C). DOD, dead of disease.

Published OnlineFirst August 18, 2010; DOI:10.1158/1078-0432.CCR-09-2660



254) and 17.7% (45 of 254) of the cases, respectively, in keeping with the high occurrence reported in previous studies (6, 8–10, 17). No focal low copy number gains were detected for *ALK*. In cases with partial 2p gain, the extra chromosomal segments varied in size from 15 to 87 Mb and included the *MYCN* gene except for one case. In the latter, *MYCN* amplification was present together with a more distal 15 Mb gain with a telomeric breakpoint immediately proximal to the *ALK* locus (Supplementary Fig. S3). The *ALK* gene was included in all except four cases of partial 2p gain (91.8%). An interesting observation, particularly in view of the high frequency of *ALK* copy number gain, was that 2p gains encompassing the *ALK* locus were present in only 2 of 17 mutated tumors (11.8%), indicating that 2p gain is not a common mechanism for increasing mutated *ALK* copy number.

To evaluate the possible impact of *ALK* copy number gain on *ALK* expression, we compared Affymetrix exon array expression data and arrayCGH data for 101 neuroblastomas. This showed a strong correlation between copy numbers of the *ALK* gene and expression levels (Spearman correlation coefficient, 0.308; $P = 0.002$; one *ALK*-amplified sample was omitted from this analysis; Supplementary Fig. S4). This was confirmed by Mann-Whitney analysis comparing the expression in tumors with normal *ALK* copy number versus tumors with *ALK* gain (CGH result >0.3; $P = 0.001$).

Next, we evaluated the relation between *ALK* gene expression and survival. We analyzed expression levels in three independent datasets including a total of 440 tumor samples (14).[16] Each analysis was done on samples profiled on one particular platform. These showed a correlation of *ALK* gene expression with survival in the global patient population (log-rank *P* values for overall and progression-free survival <0.05; Fig. 3A-C). Multivariate logistic regression analysis (in a model testing *MYCN* status, age, stage, and *ALK* expression) could show an independent prognostic value for *ALK* mRNA expression in the larger dataset (ref. 14; odds ratio, 2.94; 95% confidence interval, 1.29-6.69; $P = 1.02E-2$), but this could not be confirmed in the other two smaller datasets.

### ALK immunoreactivity

In addition to the relation between *ALK* transcript expression and survival, we also investigated the ALK protein expression status and patient survival using a tissue microarray containing 70 primary tumors. Kaplan-Meier and log-rank analysis show a significant correlation between ALK protein expression and overall survival (OS; $P = 0.014$) and progression-free survival (PFS; $P = 0.002$; Fig. 4). The three cases with *ALK* mutation (R1275Q) present on the tissue microarray had a median expression value (score 2) whereas in the remaining *ALK* wild-type tumors, ALK reactivity varied from low (score 0) to high (score 3).

For the evaluation of ALK activity, the level of activated/phosphorylated ALK (p-ALK) was investigated. However, as the specificity of p-ALK antibodies remains to be determined, we carried out Western blot analysis rather than immunohistochemistry experiments on a panel of 22 neuroblastoma cell lines. This allowed for comparison of *ALK* mRNA expression levels ($P = 0.011$) and native ALK protein levels ($P = 1.55E-07$) versus p-ALK protein level. We clearly show a significant correlation between both *ALK* mRNA expression levels and native ALK protein levels with p-ALK protein levels (Supplementary Fig. S5). Interestingly, we could also show that cell lines harboring the F1174 mutation (except for the SK-N-SH cell line with very low ALK expression levels) or *ALK* amplification have relatively more phosphorylated ALK than do cell lines with the other hotspot mutation. Moreover, cell lines with wild-type ALK have very low levels of phosphorylated ALK (Supplementary Figs. S6 and S7).

### Transforming capacity of *ALK* hotspot mutations

Given the observed concordance between mutation type and ALK activity, we also compared the transforming capacity of both *ALK* hotspot mutations in IL-3–dependent Ba/F3 cell lines.

Although both mutants were able to transform Ba/F3 cells to IL-3–independent growth, cells expressing *ALK* F1174L transformed the cells significantly faster than did Ba/F3 cells expressing *ALK* R1275Q (Fig. 5).

## Discussion

The present meta-analysis of *ALK* mutations of 709 neuroblastomas in relation to genomic profiles and clinical parameters resulted in a number of new important observations. First, substitutions at residue F1174, one of the two hotspot mutations, were significantly overrepresented in *MYCN*-amplified tumors. Moreover, patients with the F1174 mutation present with a particularly poor outcome. Second, our results indicate that, although both hotspot mutations have constitutive ALK phosphorylation, the F1174L mutation has stronger autophosphorylation and transformation capacity of Ba/F3 cells than does the R1275Q mutation. Third, in contrast to some previous reports, we show that *ALK* mutations also occur in a significant proportion of tumors with favorable stages 1, 2, and 4S (5.7% versus 7.5% in stage 3 and 4 tumors). Fourth, we show that copy number gain of the chromosome 2 region encompassing *ALK* is associated with an increased *ALK* expression. Fifth, increased *ALK* expression is associated with a worse outcome in the global population. Finally, we show that chromosome 2p is not frequently gained in tumors with *ALK* mutations, indicating that mutated *ALK* alleles are not selected for high expression by copy number gain.

The functional relevance of the high proportion of F1174 mutations in the subset of *MYCN*-amplified *ALK*-mutated neuroblastomas remains undetermined, but their co-occurrence may suggest a cooperative effect between

[16] Koster et al., submitted.

Published OnlineFirst August 18, 2010; DOI:10.1158/1078-0432.CCR-09-2660



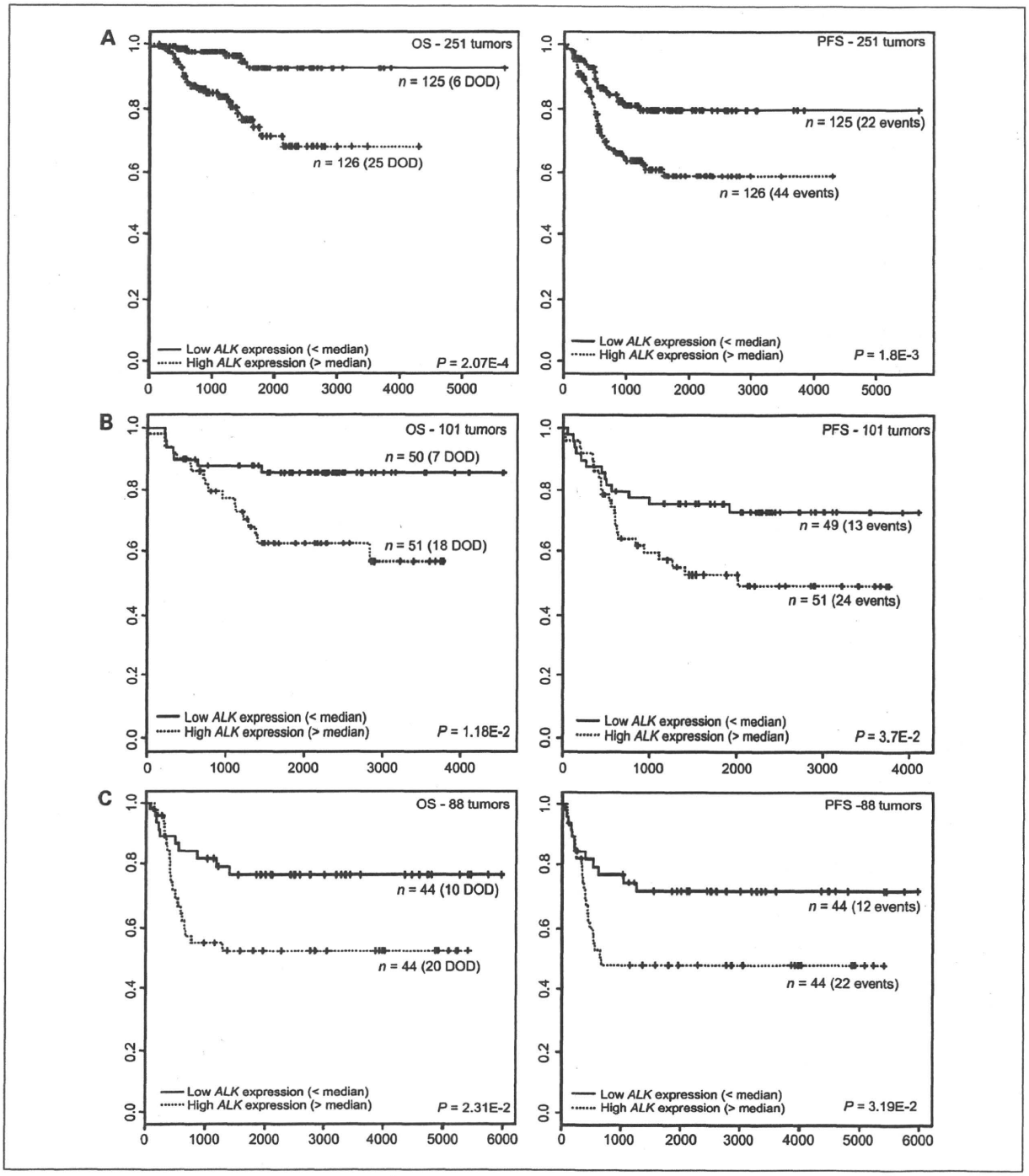


**Fig. 3.** Kaplan-Meier and log-rank analysis for overall (OS) and progression free survival (PFS) comparing tumors with high and low *ALK* mRNA expression in a published set of 251 neuroblastoma tumors (A; ref. 14), and in unpublished sets of 101 (B) and 88 (C) neuroblastoma tumors.

both aberrations in these tumors. The F1174 mutation might contribute to an additional growth and survival benefit in *MYCN*-amplified neuroblastoma cells, which may explain the particularly poor survival of these patients. The fact that neuroblastoma cell lines with *MYCN* amplifications have a relatively high frequency of F1174 mutations might also point at a particular growth advantage that may have facilitated *in vitro* growth of these cells.

Published OnlineFirst August 18, 2010; DOI:10.1158/1078-0432.CCR-09-2660



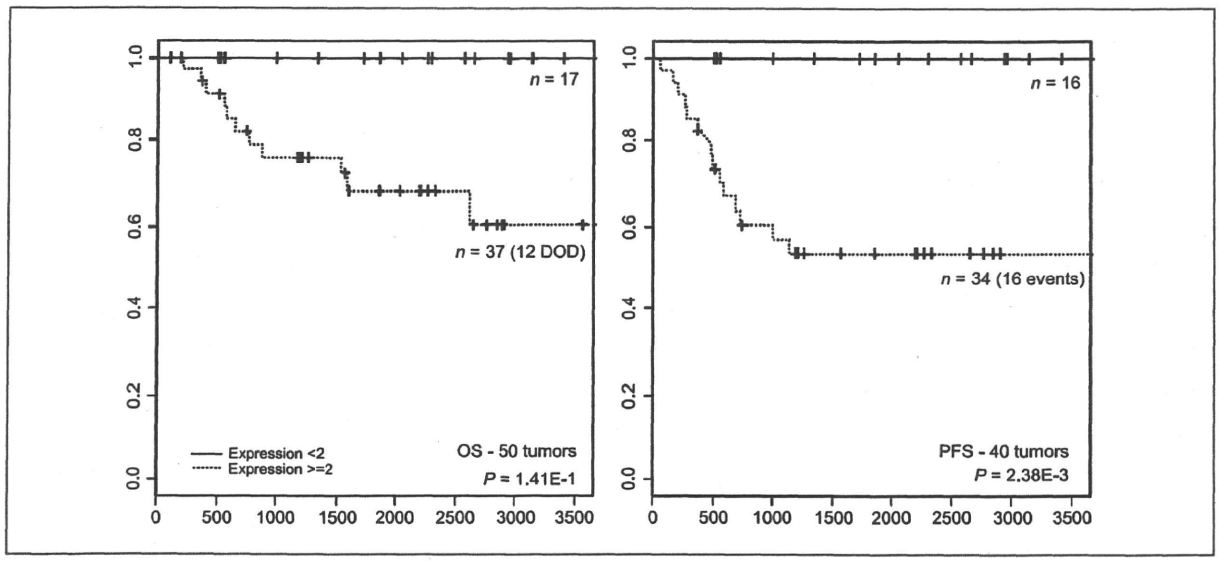


Fig. 4. Kaplan-Meier and log-rank analysis for overall (OS) and progression free survival (PFS) comparing tumors with high (expression ≥2) and low (expression <2) ALK protein expression. *X*-axis, number of days.

Of further interest in this context is the observation that F1174 mutations in the germline have not been reported up to now, which could suggest embryonic lethality. Of particular interest was the observation that only 1 of the 10 patients with *MYCN* amplification together with a F1174 mutation survived, in contrast to a 32% 5-year overall survival rate in patients with *MYCN*-amplified tumors without the F1174 mutation.

The different distribution across the genomic subtypes and the adverse impact of the F1174 mutations on survival raise the question of whether the F1174 and R1275 mutations may execute distinct effects on tumor biology. George and colleagues have previously also shown that both F1174L and R1275Q mutants could transform Ba/F3 cells, but their analysis did not reveal major differences in oncogenic potential between these two mutants, in part because the proliferation data were not reported in detail (7). In our hands, the F1174L mutant transformed the Ba/F3 cells more efficiently than did the cells expressing the R1275Q mutant. This correlated with higher autophosphorylation levels of ALK F1174L, which was not observed for the R1275Q mutant.

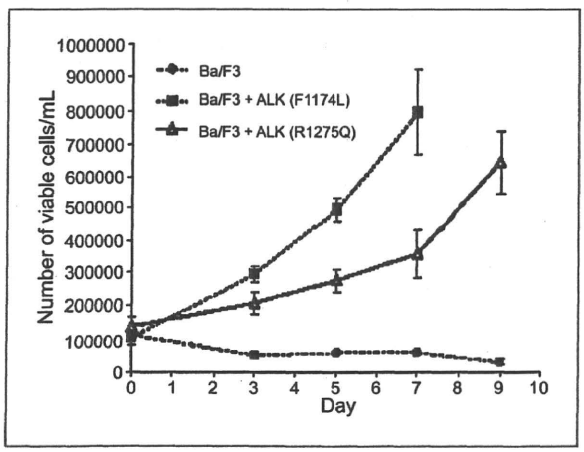


Fig. 5. Proliferation curve of Ba/F3 cells stably expressing the F1174L or R1275Q ALK mutants. Ba/F3 cells expressing mutant *ALK* as well as parental Ba/F3 cells were grown in the absence of IL-3 for a period of 9 days. A day 9 value for ALK F1174L was not included in the figure because the culture had reached maximal density before this time point.

The occurrence of mutations of particular genes in relation to genomic subgroups has been reported in certain tumor entities, such as *PIK3CA* mutations in head and neck squamous carcinomas without *EGFR* amplification and β-catenin mutations in medulloblastomas with loss of chromosome 6 (18–20). However, to the best of our knowledge, a different distribution for mutations within the same functional domain of one specific gene, as observed here for the F1174 mutation in *ALK*, has not been reported.

Our study also showed, in contrast to some of the initial studies, that *ALK* mutations occur in fairly equal frequency in both low- and high-stage tumors. Therefore, mutation analysis should also be done in patients with low-stage tumors, and the clinical characteristics and behavior of such tumors should be carefully monitored in further studies.

In addition to mutations, *ALK* activation can also result from high level gene amplification as shown by previous studies (8–10). Meta-analysis showed that this is a recurrent but rare mechanism, detected in only 1.7% of the cases. In keeping with previous studies, amplification of *ALK* almost exclusively occurs in *MYCN*-amplified tumors. Apart from such rare *ALK* high-level amplification, high-stage

Published OnlineFirst August 18, 2010; DOI:10.1158/1078-0432.CCR-09-2660



neuroblastoma tumors often exhibit gain of a large part of 2p that mostly encompasses the *ALK* locus. In our cohort, mutation analysis showed that only a minority of tumors with 2p gain carried *ALK* mutations, although 2p gains are present in as much as 19.3% of all neuroblastomas with segmental imbalances. This observation indicates that 2p gain does not act as a mechanism for increased copy number of mutated *ALK*, in contrast to what has been described for other oncogenes in other tumor entities (21, 22). In view of the variability of centromeric break points for 2p gains but almost consistent presence of *ALK* in these segments, one could assume that low copy number gain of *ALK* could also imply a growth or survival advantage for neuroblastoma cells. To test this hypothesis we analyzed the relation between *ALK* copy number and expression and the impact of increased *ALK* gene expression on survival. *ALK* gene expression was indeed shown to be copy number sensitive, and increased *ALK* expression correlated with poor survival. Using immunostaining, Passoni et al. (2009) recently showed that ALK overexpression correlated with patient survival although no correlation was found between mRNA and protein expression in their tumor cohort (23), which is in contrast with our observations in cell lines. Our findings, together with those of Passoni et al. (2009), indicate that increased ALK expression might be functionally relevant. Therefore, patients with increased ALK expression might benefit from future clinical trials with ALK inhibitors.

In conclusion, this meta-analysis shows for the first time that the recurrent F1174 mutation predominantly occurs in *MYCN*-amplified tumors, and clearly shows differences in the frequency and distribution of *ALK* mutations across the different genomic subtypes in neuroblastoma. The F1174 mutation might suggest a poor prognosis in patients with *MYCN* amplification, but further studies are needed to substantiate this hypothesis. Furthermore we could show that the F1174L mutant displayed a higher degree of ALK phosphorylation and tumorigenicity than did the R1275Q mutant. No significant difference was observed in the frequency of *ALK* mutations between low- and high-stage tumors.

## Disclosure of Potential Conflicts of Interest

No potential conflicts of interest were disclosed.

## Acknowledgments

We thank Justine Nuytens for excellent technical support.

## Grant Support

EU under FP6 (EET-pipeline, nr.037260 and the Kids Cancer Kinome program, nr.6037390), FWO (G.0198.08), IWT (SBO60848), GOA (01G01910). This article presents research results of the Belgian program of Interuniversity Poles of Attraction, initiated by the Belgian State, Prime Minister's Office, Science Policy Programming, Methusalem-program [BOF08/01M01108], FOD (NKP_29_014), Stichting Kindergeneeskundig Kankeronderzoek, the KIKA Foundation. K. De Preter is postdoctoral researcher with the FWO. R. Noguera is supported by ICIII RD06/0020/0102. C. Kumps and M. Porcu are supported by the IWT, J. Cools and P. Zabrocki are supported by Foundation against Cancer (SCIE2006-34, J.C.) and J. Hoebeeck is a postdoctoral research supported by a grant of the Ghent University (BOF01P07406) and by the fund for Scientific Research Flanders (KAN1.5.207.08).

The costs of publication of this article were defrayed in part by the payment of page charges. This article must therefore be hereby marked *advertisement* in accordance with 18 U.S.C. Section 1734 solely to indicate this fact.

Received 10/02/2009; revised 05/19/2010; accepted 07/13/2010; published OnlineFirst 08/24/2010.

## References

1. Maris JM, Hogarty MD, Bagatell R, Cohn SL. Neuroblastoma. Lancet 2007;369:2106–20.
2. Vandesompele J, Baudis M, De Preter K, et al. Unequivocal delineation of clinicogenetic subgroups and development of a new model for improved outcome prediction in neuroblastoma. J Clin Oncol 2005;23:2280–99.
3. Michels E, Vandesompele J, De Preter K, et al. ArrayCGH-based classification of neuroblastoma into genomic subgroups. Genes Chromosomes Cancer 2007;46:1098–108.
4. Janoueix-Lerosey I, Schleiermacher G, Michels E, et al. Overall genomic pattern is a predictor of outcome in neuroblastoma. J Clin Oncol 2009;27:1026–33.
5. Brodeur GM. Molecular basis for heterogeneity in human neuroblastomas. Eur J Cancer 1995;31A:505–10.
6. Mosse YP, Laudenslager M, Longo L, et al. Identification of ALK as a major familial neuroblastoma predisposition gene. Nature 2008;455:930–5.
7. George RE, Sanda T, Hanna M, et al. Activating mutations in ALK provide a therapeutic target in neuroblastoma. Nature 2008;455:975–8.
8. Chen Y, Takita J, Choi YL, et al. Oncogenic mutations of ALK kinase in neuroblastoma. Nature 2008;455:971–4.
9. Caren H, Abel F, Kogner P, Martinsson T. High incidence of DNA mutations and gene amplifications of the ALK gene in advanced sporadic neuroblastoma tumours. Biochem J 2008;416:153–9.
10. Janoueix-Lerosey I, Lequin D, Brugieres L, et al. Somatic and germline activating mutations of the ALK kinase receptor in neuroblastoma. Nature 2008;455:967–70.
11. Brodeur GM, Pritchard J, Berthold F, et al. Revisions of the international criteria for neuroblastoma diagnosis, staging, and response to treatment. J Clin Oncol 1993;11:1466–77.
12. Menten B, Pattyn F, De Preter K, et al. arrayCGHbase: an analysis platform for comparative genomic hybridization microarrays. BMC Bioinformatics 2005;6:124.
13. Olshen AB, Venkatraman ES, Lucito R, Wigler M. Circular binary segmentation for the analysis of array-based DNA copy number data. Biostatistics 2004;5:557–72.
14. Oberthuer A, Berthold F, Warnat P, et al. Customized oligonucleotide microarray gene expression-based classification of neuroblastoma patients outperforms current clinical risk stratification. J Clin Oncol 2006;24:5070–8.
15. Shimada H, Ambros IM, Dehner LP, Hata J, Joshi VV, Roald B. Terminology and morphologic criteria of neuroblastic tumors: recommendations by the International Neuroblastoma Pathology Committee. Cancer 1999;86:349–63.
16. Lierman E, Michaux L, Beullens E, et al. FIP1L1-PDGFRalpha D842V, a novel panresistant mutant, emerging after treatment of FIP1L1-PDGFRalpha T674I eosinophilic leukemia with single agent sorafenib. Leukemia 2009;23:845–51.
17. Spitz R, Oberthuer A, Zapatka M, et al. Oligonucleotide array-based

Published OnlineFirst August 18, 2010; DOI:10.1158/1078-0432.CCR-09-2660



comparative genomic hybridization (aCGH) of 90 neuroblastomas reveals aberration patterns closely associated with relapse pattern and outcome. Genes Chromosomes Cancer 2006;45:1130–42.
18. Clifford SC, Lusher ME, Lindsey JC, et al. Wnt/Wingless pathway activation and chromosome 6 loss characterize a distinct molecular sub-group of medulloblastomas associated with a favorable prognosis. Cell Cycle 2006;5:2666–70.
19. Fattet S, Haberler C, Legoix P, et al. β-Catenin status in paediatric medulloblastomas: correlation of immunohistochemical expression with mutational status, genetic profiles, and clinical characteristics. J Pathol 2009;218:86–94.
20. Murugan AK, Hong NT, Fukui Y, Munirajan AK, Tsuchida N. Oncogenic mutations of the PIK3CA gene in head and neck squamous cell carcinomas. Int J Oncol 2008;32:101–11.
21. Zatkova A, Merk S, Wendehack M, et al. AML/MDS with 11q/MLL amplification show characteristic gene expression signature and interplay of DNA copy number changes. Genes Chromosomes Cancer 2009;48:510–20.
22. Hu G, Chong RA, Yang Q, et al. MTDH activation by 8q22 genomic gain promotes chemoresistance and metastasis of poor-prognosis breast cancer. Cancer Cell 2009;15:9–20.
23. Passoni L, Longo L, Collini P, et al. Mutation-independent anaplastic lymphoma kinase overexpression in poor prognosis neuroblastoma patients. Cancer Res 2009;69:7338–46.

Cancer Science
The official journal of the Japanese Cancer Association JCA

*Review Article*

# Global genomic and RNA profiles for novel risk stratification of neuroblastoma

**Miki Ohira[1,2] and Akira Nakagawara[1,3]**

[1]Division of Biochemistry and Innovative Cancer Therapeutics, [2]Laboratory of Cancer Genomics, Chiba Cancer Center Research Institute, Chuoh-ku, Chiba, Japan

(Received March 31, 2010/Revised July 8, 2010/Accepted July 9, 2010/Accepted manuscript online July 16, 2010/Article first published online August 20, 2010)

**Neuroblastoma is one of the most common solid tumors in children. Its clinical behavior ranges widely from spontaneous regression to life-threatening aggressive growth. The molecular etiology of neuroblastoma is still enigmatic and the overall cure rate of advanced disease is still very poor. Recent microarray-based technology provided us with important information such as comprehensive genomic alterations and gene expression profiles to help us understand the molecular characteristics of each tumor in detail. Several retrospective studies have revealed that these signatures are strongly correlated with patient prognoses and led to the construction of new risk stratification systems, some of which are considered for evaluation in upcoming clinical studies in a prospective way. Large-scale analyses using a variety of genetic tools also discovered a major familial neuroblastoma predisposition gene *ALK*, as well as new candidate susceptibility genes at 6q22 and 2q35 for sporadic neuroblastoma. Of note, *ALK* is mutated in 6–9% of sporadic cases, and is either amplified or constitutively activated through mutations mainly within the kinase domain, promoting the possibility of new therapeutic strategies using ALK inhibitors. Additional candidates for outcome predictors such as the methylation phenotype of tumor DNA and expression profiles of microRNA have also been proposed. Such variety of information will help us understand the heterogeneity of neuroblastoma biology and further, the combined use of these signatures will be beneficial in predicting prognosis with high accuracy, as well as choosing a suitable therapy for the individual patient. (*Cancer Sci* 2010; 101: 2295–2301)**

Neuroblastoma is one of the most common pediatric solid tumors, which accounts for 15% of all pediatric cancer deaths. It originates from the sympathoadrenal lineage derived from the neural crest and clinical behavior is markedly heterogeneous.[1] Tumors found in patients under 1 year of age are mostly favorable and often show spontaneous differentiation or regression, whereas tumors found in patients over 1 year of age tend to grow aggressively and often have a fatal outcome.[1] Recent development of chemotherapy has dramatically increased the survival rates of many pediatric cancers; however, advanced stage neuroblastoma, especially those with genomic amplification of the *MYCN* oncogene, are frequently resistant to any therapy and the outcome for patients is still very poor.[1,2]

Table 1 shows the 10-year survival rates for patients in each stage whose tumors were clinically found in Japan and sent to Chiba Cancer Center Research Institute from 1995 to 2007. In our dataset, *MYCN*-amplified cases ($n$ = 83) showed only a 29% long-term survival rate despite intensive multimodal therapy, while *MYCN* non-amplified cases ($n$ = 260) displayed 65% survival. Furthermore, part of the neuroblastomas categorized in the intermediate-risk group (stage 3 or 4 tumors that possess a single copy of the *MYCN* gene) often recur after a complete response to the initial therapy. Such differences in the final outcome of patients with neuroblastoma are presumably considered attributable to differences in the genetic and biological characteristics that are reflected in the gene and protein expression profiles of the tumor.

Thus, neuroblastoma is still one of the most challenging tumors to treat. A better understanding of the molecular characteristics of neuroblastoma and a novel therapeutic strategy, which is most effective for each tumor subset, combined with precise tumor risk classification are required for improvement of the cure rate, as well as the quality of life of the patients. In this review, we summarize recent efforts to construct a novel tumor-risk stratification system for neuroblastoma based on the latest genome-wide genetic and gene expression profiling assays.

## Conventional risk markers for neuroblastoma

Early studies based on cytogenetics have presented several prognostic markers such as DNA ploidy,[3] *MYCN* amplification,[4,5] and gains of chromosome arms 1q, 2p and 17q, as well as allelic losses of 1p, 3p and 11q.[6,7] Many gene expression markers have also been reported so far through comparison between neuroblastoma subsets with good and poor prognosis,[8,9] or based on neuronal functions; the genes whose mRNA expression is high in the favorable type of neuroblastoma include *TRKA*, *CD44*, *pleiotrophin*, *N-cadherin*, *H-RAS*, *ECEL1*, *NLRR3*, *BMCC1*, *NEDL1* and *ZNF423*,[10–18] and those in the unfavorable ones include *TRKB*, *TERT*, *CDC10*, *NLRR1*, *HEN2* and *LMO3*.[10,19–22] Several positional candidate genes such as *SVV/BIRC5*, *NM23-H1* and *NM23-H2* and *PPM1D* on 17q, whose expression levels are higher in advanced neuroblastomas, have also been identified.[23–26] Similarly, *TSLC1/IGSF4/CADM1*, which is mapped to 11q and known as a tumor suppressor gene for lung cancer, showed lower expression in advanced neuroblastomas.[27,28]

Gene function-based approaches identified several important signaling pathways strongly affecting tumor progression and treatment resistance. In addition to the Trk family, the PI3K/Akt pathway, Ret, HGF/c-Met pathway and Src family kinases such as Fyn and Shc family were reported to be closely associated with several prognostic factors and biological characteristics of neuroblastoma cells.[29–32] Because *MYCN* amplification is a strong poor prognostic factor, many researchers have been interested in searching for the genes transcriptionally regulated by the MYCN transcription factor to understand the molecular

[3]To whom correspondence should be addressed. E-mail: akiranak@chiba-cc.jp

doi: 10.1111/j.1349-7006.2010.01681.x

**Table 1. Long-term survival rates of neuroblastoma in each international neuroblastoma staging system (INSS) stage**

| INSS stage | No. patients | Survival† (%) | *MYCN* amplification |
|---|---|---|---|
| 1 | 48 | 100 | 0 |
| 2 | 29 | 92.6 | 3 |
| 3 | 60 | 70.4 | 14 |
| 4 | 179 | 33.3 | 64 |
| 4s | 27 | 59.3 | 2 |
| Total | 343 | | 83 |

†Ten-year survival rate.

characteristics in tumors with and without *MYCN* amplification.[33,34]

Thus, certain numbers of markers have been proposed; however, each single marker has still not been sufficient to be newly included in clinical practice. Therefore, current clinical studies using many divergent therapeutic strategies have adopted only limited clinical markers with a strong prognostic impact, including: patient age at diagnosis with two age cut-offs of 12 and 18 months;[35,36] disease stage defined by the international neuroblastoma staging system (INSS);[37] *MYCN* copy number and 1p loss; and sometimes add DNA ploidy and histopathological information[38] for risk stratification (US, Europe and Japan). To make an efficient tumor classification system, multiple genes that explain each character of tumor subsets need to be considered in a computational machine-learning approach that is recently sophisticated for cancer study.

## Risk classification of neuroblastoma by gene expression signatures

Microarray technology enabled us to examine simultaneously enormous molecular features including gene expression and genome alterations in tumors and to construct a novel prognosis classifier by using those with high performance. One of the good practical examples is the 70 genes-based risk classification system for breast cancer, which was approved by the FDA as the first microarray-based biomarker for cancer diagnosis.[39] As for neuroblastoma, the study by Wei *et al.*[40] for the first time indicated that a gene-expression-based classifier can predict the prognosis of patients efficiently by profiling the 56 tumors using cDNA microarrays containing 42 578 cDNA clones (classification accuracy was 95% for 21 test samples).

We also conducted gene expression analysis of 136 neuroblastomas diagnosed in Japan by using a 5340 neuroblastoma-derived genes chip.[41] The top-ranked 70 prognosis-related genes were selected through machine learning with the survival information of patients and used to construct a computational algorithm for prognosis prediction. The algorithm calculates survival probabilities of each patient at 2 years or 5 years after diagnosis, which is indicated by a "*posterior*" value range from 0 to 1 (Fig. 1). The microarray classifier could predict patient prognosis with high efficiency (90% accuracy, 96% sensitivity and 90% specificity), and is revealed to be the only powerful predictor to classify intermediate-risk-type neuroblastoma (stage 3 or 4 without *MYCN* amplification, prediction accuracy was 86%), whereas the current clinical markers (age, stage and *MYCN*) exhibited only 64% accuracy.

Based on these results, we subsequently made a "mini-chip" carrying the top-ranked 200 genes for clinical use.[41] The independent test of 50 tumor samples for evaluation indicated high reproducibility as well as high efficiency (approximately 89%) for our chip system. This mini-chip test is now under clinical validation in a larger cohort in Japan. This work is the first to construct a clinically available DNA chip harboring prognosis-related genes specifically selected for prognosis prediction, which gave a highly reproducible result to those obtained by the chip for the original screening.

Oberthuer *et al.*[42] then indicated that the gene expression classifier may improve the risk estimation of current neuroblastoma trials. By using a customized oligonucleotide microarray comprising 10 163 probes, they constructed a 144-gene predictor from 77 samples, which could classify 174 patients more accurately than risk stratification of current trials from Germany, Japan and the United States ($P < 0.001$).

Asgharzadeh *et al.*[43] focused their work on 102 intermediate-risk neuroblastomas (with *MYCN* nonamplified stage 4 disease) using Affymetrix arrays containing 45 000 probes. This work describes the first gene-expression-based classifier specifically generated for metastatic neuroblastoma lacking *MYCN* amplification.

Although the precision and reproducibility of microarray analysis have been markedly improved, validation of microarray data obtained by different platforms has been necessary to evaluate selected genes using an independent technology such as quantitative real-time PCR (qPCR). Schram *et al.*[44] first applied the multiplex qPCR method to have their gene-expression-based classifier from 63 neuroblastoma patients. They showed qPCR was almost comparable, although with some exceptions, with results obtained using the Affymetrix platform, and that multiplex qPCR could provide a convenient and less expensive tool for routine application in a clinical setting.

To select reliable genes that will provide a stable prediction result to make better risk classification, meta-analysis of previously reported studies have also been conducted.[45,46] Chen *et al.*[45] compared the gene expression profiles of 42 neuroblastoma samples using both cDNA and the Affymetrix platforms and concluded that gene expression studies performed in different platforms could be integrated for prognosis analysis after removing the variation resulting from the different platforms. Quite recently, Vermeulen *et al.*[46] selected 59 genes as a prognosis classifier based on a re-analysis of seven published microarray gene expression studies combined with previously reported single-candidate prognostic genes, and conducted a large-scale retrospective study by applying qPCR to 30 training samples, 313 test samples and 236 blind validation samples. Their multigene-expression signature exhibited 85.4% accuracy, 84.4% sensitivity and 86.5% specificity for those samples.

## Risk classification of neuroblastoma by genomic signatures

In the 1990s, loss of heterozygosity, fluorescence *in situ* hybridization, and comparative genomic hybridization (CGH) analyses have been used for detecting the chromosome alterations that occurred in neuroblastoma with approximately several ten megabases of resolution. From the 2000s, microarray-based technology combined with the CGH method (array CGH) enabled us to obtain genome-wide, high-resolution genomic information simultaneously (from 1 megabase to <10 kilobases). Early studies have used in-house bacterial artificial chromosome (BAC) array or cDNA microarray to identify novel cancer-related genes or crucial genome copy number alterations that determine distinct genetic subgroups for risk stratification.[47,48] Recent array CGH studies also strongly support the idea that neuroblastoma tumors can be categorized by the genomic signature into several subgroups with different alteration patterns and prognosis. To unveil DNA copy number alterations that characterize distinct subsets of neuroblastoma, we have conducted array CGH with a DNA chip carrying 2464 BAC clones (whose resolution was approximately 1 Mb) to examine genomic aberrations in 236 primary neuroblastomas in Japan (112 sporadic and 124 mass screening cases, Fig. 2).[49]



doi: 10.1111/j.1349-7006.2010.01681.x

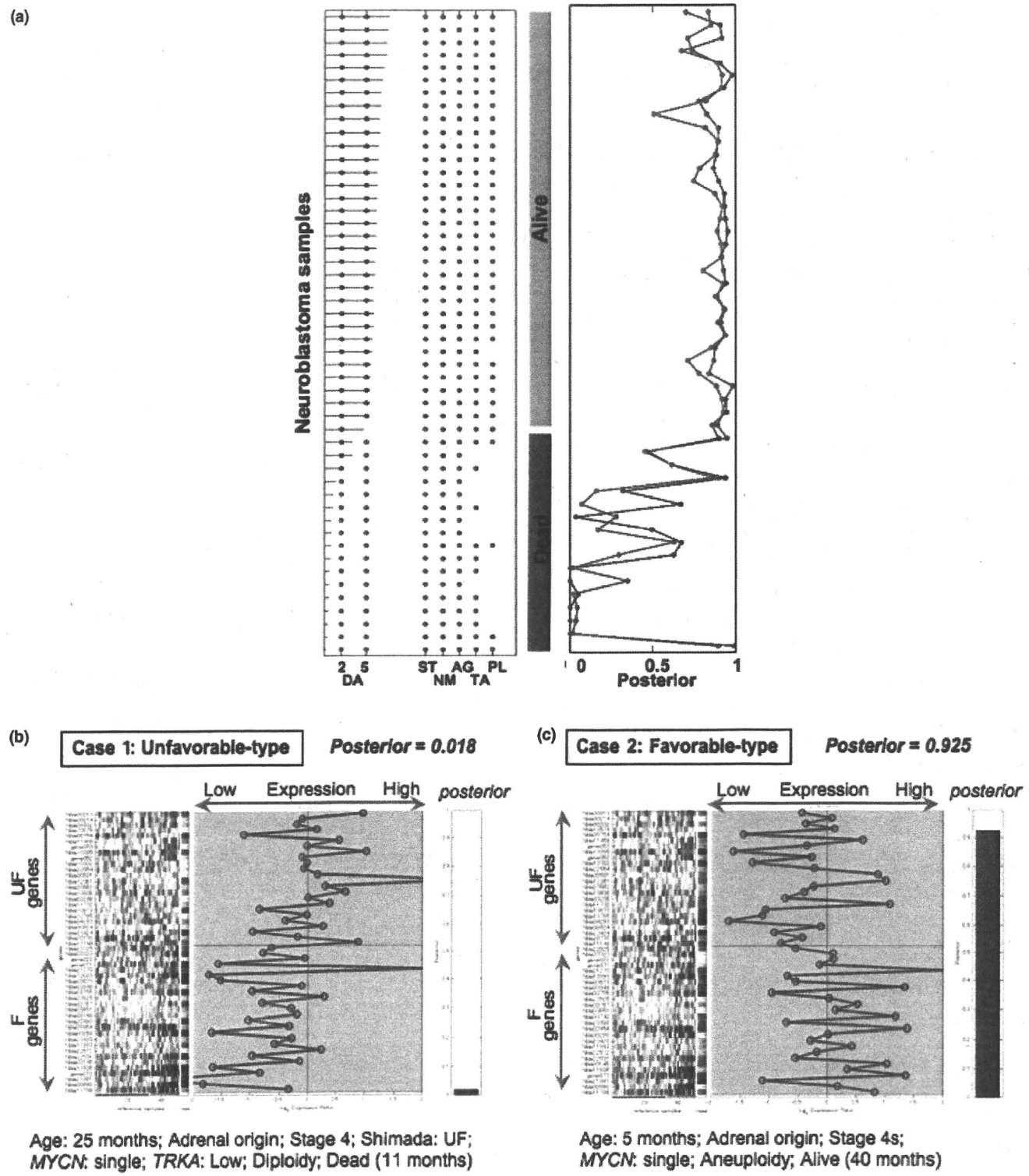


**Fig. 1.** Gene expression profile-based classifier to predict prognosis of the patient with neuroblastoma. (a) Posterior probability of survival at 5 years for 50 neuroblastomas measured by 200 genes-diagnostic mini-chip. Left panel: neuroblastoma samples with clinical information. DA, outcome (red, dead; blue, alive) at 2 years and 5 years after diagnosis; ST, international neuroblastoma staging system (INSS) stage (red, 3 or 4; blue, 1, 2 or 4s); NM, *MYCN* amplification (red, amplified; blue, not amplified); AG, age at diagnosis (red, ≥1 year; blue, <1 year); TA, *TRKA* expression (red, low; blue, high); PL, DNA ploidy (red, diploidy; blue, aneuploidy). A red or blue horizontal line denotes the survival period after diagnosis for a dead or alive patient, respectively. Right panel: prediction results when the supervised classifier constructed from 136 training samples is applied to the 50 independent samples (blue). Leave two out cross-validation analysis using the 50 samples (red). Higher value of posterior means a higher probability of a good prognosis. (b,c) Representative examples of the mini-chip test. Case 1 predicted as the unfavorable type. Posterior: 0.018. Case 2 predicted as the favorable type. Posterior: 0.925.

Our array CGH analysis demonstrated three major groups of genomic alterations in sporadic neuroblastomas ($n$ = 112) that can well define the prognoses of neuroblastomas: a genetic group (GG) of silent with no obvious losses and gains except *MYCN* amplification (GG-S, $n$ = 23; 5-year cumulative survival rate: 68%; DNA ploidy: 87% diploidy); that of partial chromosomal gains and/or losses (GG-P, $n$ = 53; 43% survival; 77% diploidy); and that of whole chromosomal gains and/or losses (GG-W, $n$ = 36; 80% survival; 22% diploidy). Further subcategorization of the three groups was based on signatures with strong correlation values to the prognosis (1p loss, *MYCN* amplification and 11q loss) resulting in several cohorts with highly contrasting outcomes (Fig. 2).

Statistical analyses of our two classifiers constructed by array CGH (GG-S, GG-P and GG-W) and gene expression profiling (*posterior* value)[41] in sporadic neuroblastomas showed that, in addition to the gene expression signature, the genomic signature is also a significant prognostic indicator for all and/or the intermediate risk-type of neuroblastoma (Table 2). More importantly, multivariate analysis indicated that these two signatures were mutually independent prognostic indicators (Table 2, bottom), especially among the patients with intermediate-risk-type tumors.[49] To validate this risk classification in a new, independent sample set, we started additional array CGH analysis by applying another genome platform (Agilent oligo-microarray and Affymetrix SNP chip) (Ohira *et al.*, manuscript in preparation).

Similarly, Janoueix-Lerosey *et al.*[50] examined 493 French patients by array CGH and indicated that analysis of the overall genomic pattern is essential to predict relapse in neuroblastoma patients. Their subclassification uses the structural alterations of "segmental" and "numerical" in addition to *MYCN* amplification. The resulting five subgroups have clearly differing outcomes. Tumors presenting exclusively numerical were associated with excellent survival, whereas the presence of segmental alterations with or without *MYCN* amplification was the strongest predictor of relapse.

In contrast to the gene expression microarray analysis, array CGH technology needs smaller amount of tumor materials and provides highly reproducible data even if different kinds or a lot of platforms are used. Considering that the gene expression signature and the genome alteration signature were independent risk predictors,[49] prospective studies using both gene expression and array CGH signatures will really be necessary to validate each potential in risk stratification for neuroblastoma.

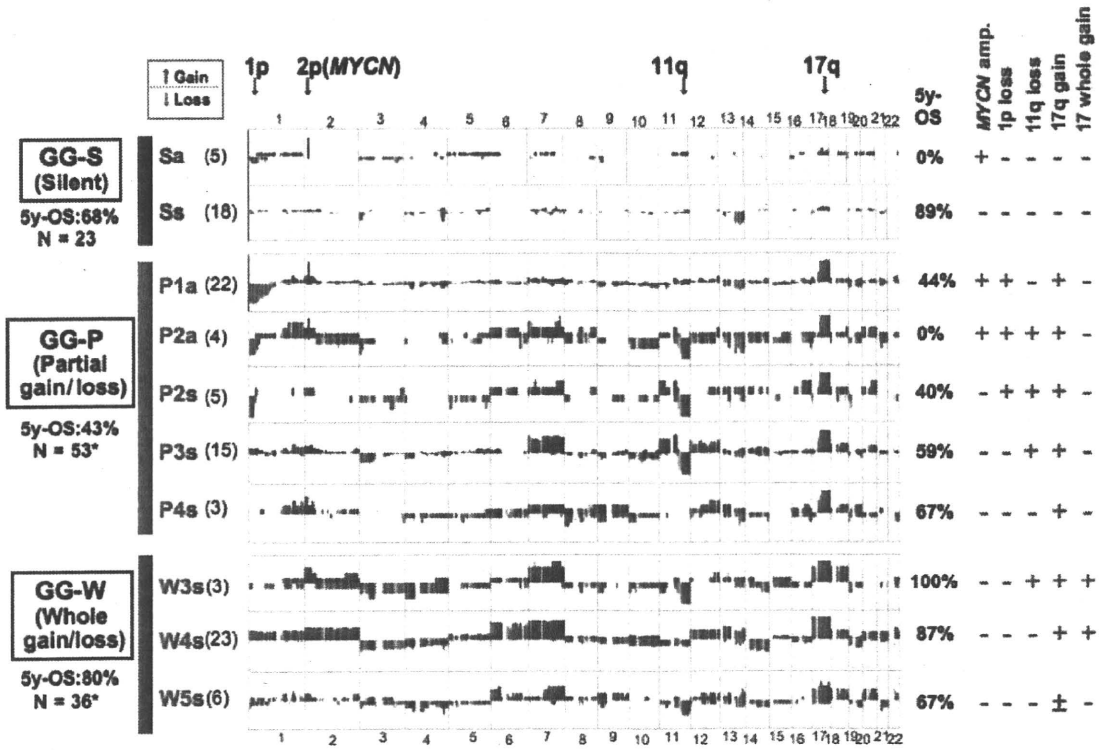


**Fig. 2.** Genome alteration-based risk classification of neuroblastoma. Representative genomic signatures of 112 sporadic neuroblastomas detected by array comparative genomic hybridization (CGH). In this figure, only the major subgroups (sample number in genomic subgroups ≥3) are shown. The panel in the middle shows 20 Mb-averaged frequencies of gains (upper panel, shown by red lines) and losses (lower panel, shown by green lines) at chromosome locations complementary to bacterial artificial chromosome (BAC) clones in each genomic subgroup. The right panel shows the 5-year overall survival rates (5y-OS), as well as the important features of chromosomal events including *MYCN* amplification, deletions of chromosomes 1p and 11q and gains of chromosome 17q or whole chromosome 17. Genomic groups (GG-S, GG-P, and GG-W) and subgroups (Sa, Ss, etc.) with the sample number involved in each group (*N*, total sample number in each genomic group; *note that only representative groups are shown) and subgroup (in parenthesis) are also indicated on the left. a, *MYCN* amplified; s, *MYCN* non-amplified. Note that GG-S, GG-P and GG-W corresponded well with the pattern of chromosome 17 abnormalities, namely, no gain of either chromosome 17 or 17q, gain of chromosome 17q and gain of whole chromosome 17, respectively. Subgroup 1 harbors 1p loss but not partial 11q loss. Subgroup 2 has both 1p and 11q losses. Subgroup 3 has partial 11q loss but not 1p loss. Subgroup 4 has no partial 1p and 11q loss. Subgroup GG-W5 is the exception and has whole chromosomal gains and losses in several chromosomes, but not whole chromosome 17 gain. GG-W subgroups showed a favorable prognosis, except for two cases with *MYCN* amplification. Sa is very poor (5y-OS: 0%), whereas Ss showed favorable prognosis (5y-OS: 89%). Patients with GG-P tumors exhibited various survival rates but a lower range, from 0% to 67%; the P2s subgroup (5y-OS: 40%) had a worse survival rate than P3s (5y-OS: 59%). It may be that 1p and 11q loss may have a similar impact on patient survival and work additively to the prognosis. Only the P1a subgroup showed a better prognosis among Pa tumors (5y-OS: 44%). For more detail, see reference 49.



doi: 10.1111/j.1349-7006.2010.01681.x

Table 2. Clinical impact of genomic and gene expression signatures, as well as other conventional prognostic factors in sporadic neuroblastomas

| | Sporadic neuroblastomas ($n$ = 112) | | | |
|---|---|---|---|---|
| | $n$ | $P$-value | HR | CI |
| Univariate analysis | | | | |
| Array CGH signature (P *versus* W + S) | 53 *vs* 59 | 0.003 | 2.6 | (1.4, 4.9) |
| Gene exp. signature (Posterior <0.5 *vs* ≥0.5) | 22 *vs* 18 | <0.001 | 11.2 | (2.5, 49.4) |
| Age at diagnosis (≥1 year old *versus* <1 year old) | 74 *vs* 38 | 0.006 | 2.7 | (1.2, 5.8) |
| INSS stage (3, 4 *vs* 1, 2, 4s) | 73 *vs* 38 | <0.001 | 4.9 | (1.9, 12.5) |
| *MYCN* (Amplification *versus* Single copy) | 36 *vs* 75 | <0.001 | 4.0 | (2.2, 7.4) |
| Multivariate analysis | | | | |
| Array CGH signature (P *versus* W + S) | 15 *vs* 25 | 0.045 | 2.9 | (1.0, 8.3) |
| Gene exp. signature (Posterior <0.5 *vs* ≥0.5) | 22 *vs* 18 | 0.002 | 7.5 | (1.7, 33.4) |

CGH, comparative genomic hybridization; CI, confidence interval; HR, hazard ratio; INSS, international neuroblastoma staging system; $n$, sample number; P, $P$-value.

## *ALK* gain-of-function mutations in familial and sporadic neuroblastoma cases

A familial history of neuroblastoma is identified in 1–2% of cases. A genome-wide scan in neuroblastoma pedigrees and subsequent resequencing of candidate loci have identified a major familial neuroblastoma predisposition gene *Anaplastic lymphoma kinase* (*ALK*).[51] Somatic *ALK* mutations or amplifications were also identified in 6–9% of sporadic cases.[52–65] ALK is a receptor tyrosine kinase predominantly expressed in the developing nervous system. Most of the ALK mutations reported so far are localized within the kinase domain and are assumed to produce constitutively activated proteins. A number of neuroblastoma cell lines were also shown to harbor activating ALK mutations. According to the recent success of small molecule tyrosine kinase inhibitors in a certain subset of cancers, such as gefitinib in non-small-cell lung carcinoma with epidermal growth factor receptor (EGFR) mutations, a similar therapeutic approach based on inhibition of ALK-mediated signaling will be expected to target oncogenic ALK mutations in neuroblastoma. Several studies using the existing ALK inhibitor compounds have shown that neuroblastoma cell lines harboring different activating ALK mutations appear to respond differently to the agent. The reasons behind this differential response to the inhibitor are currently unclear, but may indicate differences in the genetic background, or reflect complex genetic predispositions acquired by these cells.[56]

Under the current protocols, patients with *ALK* mutation or amplification appear to have a worse prognosis. However, ALK abnormalities seem to highly correlate with *MYCN* amplification, so whether *ALK* mutation is an independent risk factor for poor prognosis or not needs to be further investigated in a large cohort.[52]

Loss-of-function germ line mutations have been detected in *PHOX2B*, a homeobox gene functioning as an important regulator of normal autonomic nervous system development, implicating this pathway in neuroblastoma initiation in a certain subset of cases.[57–59] However, subsequent studies for this gene have indicated that *PHOX2B* mutations explain only a small subset of hereditary neuroblastoma and are rare in sporadic neuroblastomas.

## Genome-wide association study: risk alleles associated with malignant neuroblastoma

Since the majority of neuroblastomas arise without a family history of the disease, the hypothesis that multiple common DNA variations cooperate to increase the risk for neuroblastic malignant transformation was considered. By using a large number of samples from more than 1700 neuroblastoma patients, as well as over 4000 controls, Maris *et al.*[60,61] conducted a genome-wide association study (GWAS) of 550 000 SNP genotypes and identified common SNP alleles within the putative *FLJ22536* and *FLJ44180* genes at 6p22 and within the introns of the *BARD1* gene at 2q35, which are associated with sporadic neuroblastoma with malignant phenotypes. BARD1 is known to heterodimerize with the familial breast cancer gene product BRCA1 and is considered to be essential for the tumor suppressive function of BRCA1.

Copy number variations (CNV) have been shown to significantly influence mRNA expression levels and recent studies have described associations of CNV with some of the common diseases. Subsequent CNV-based GWAS indicated that a common CNV at 1q21.1 likewise contributes to neuroblastoma susceptibility, and that this CNV leads to an altered expression of *NBPF23*, a new member of the neuroblastoma breakpoint family (NBPF) genes.[62]

Ongoing studies are now focused on understanding the biological consequences of these common DNA variations in the developing sympathetic neuroblast and how these influence malignant transformation.

## Epigenetic alterations

Recently, epigenetic alterations have been reported to be strongly related to the patient prognosis with neuroblastoma. Methylation of CpG islands (CGI), which is deeply involved in embryonic development and tissue differentiation, is one of the epigenetic alterations in cancer. According to early studies, promoters such as *RASSF1A*, *CASP8*, *BLU* and *DCR2* genes, were frequently hypermethylated in primary neuroblastomas and neuroblastoma cell lines.[63]

Abe *et al.*[64–66] first proposed that CpG island methylator phenotype (CIMP) in the tumor genome, which is defined sensitively by five CGI such as the *Protocadherin beta* family, is strongly associated with poor survival of patients with neuroblastoma with extremely high hazard ratios, reaching as high as 22 and 9.5 in Japanese and German cases, respectively. Strikingly, the CIMP was also a significant and strong prognostic marker among the cases without *MYCN* amplification.[65,66]

Very recently, a sensitive method to detect methylation of *RASSF1A* and *DCR2* promoters in circulating tumor-originated genomic DNA in serum has been developed.[67,68] Hypermethylation of these genes is strongly correlated with poor prognosis. This technique will also be available for other systems like genome copy number changes in the near future, so the diagnosis and risk classification of neuroblastoma will be quicker and less stressful for patients.

## Expression profiles of non-coding RNA also correlate the neuroblastoma subtypes

MicroRNA (miRNA) is a class of small non-coding RNA that regulates gene expression at a post-transcriptional level.[69,70] Its deregulation has recently been implicated in the pathogenesis of neuroblastoma. For instance, miR-34a on chromosome 1p acts as a suppressor of oncogene in neuroblastoma,[71–73] whereas some miRNA, such as miR-17-5p, OncomiR-1 and miR-9, behave like oncogenes or metastasis-promoting genes through direct up-regulation by MYCN.[74–76] Expression profiling studies of miRNA have identified a set of miRNA that are differentially expressed between favorable and unfavorable tumor subtypes of neuroblastoma[74,76–78] and these expression profiles were also predicative of the clinical outcome, highlighting the potential for miRNA-mediated diagnostics and therapeutics. Bray and co-workers analyzed 145 neuroblastomas for miRNA expression (430 loci) by stem-loop RT qPCR.[79] They developed a signature from 15 miRNA that was predictive of overall survival with 73% sensitivity and 87% specificity in the 49 validation set of tumors.

The large non-coding RNA are another class of non-coding RNA that are usually produced by RNA polymerase II and lack a significant open-reading frame.[70] We have identified *ncRAN*, a novel large non-coding RNA transcript whose higher expression significantly correlated with a poor prognosis of patients ($P = 0.0002$), and was recognized as an independent prognostic factor from age, disease stage and *MYCN* expression.[80] Because a certain number of such long non-coding cDNA have been observed in our neuroblastoma cDNA library,[8,9,41] further analysis of such clones will be necessary to examine the role of long non-coding RNA in neuroblastoma biology.

## Future directions

The era of personalized medicine is likely to see an escalation in the use of biomarkers to ensure cancer patients receive optimal treatment. Microarray contents are still getting more variations with higher resolution (genomes, SNP, transcripts, miRNA and proteins). In addition, new generation DNA sequencing technologies have been developed rapidly. In the next few years, we will have a lot of information about mutations of oncogenes and tumor suppressors, as well as detailed mRNA expression profiles to be integrated into future personalized medicine for neuroblastoma. Data obtained by these technologies will facilitate our understanding for the mechanism of heterogeneity in the clinical phenotype. The integration of multiple molecular profiles after sufficient validation by multivariate-statistical analyses will make tumor risk classification for neuroblastoma much more feasible.

## References


1 Brodeur GM. Neuroblastoma: biological insight into a clinical enigma. *Nat Rev Cancer* 2003; **3**: 203–16.
2 Maris JM. The biologic basis for neuroblastoma heterogeneity and risk stratification. *Curr Opin Pediatr* 2005; **17**: 7–13.
3 Look AT, Hayes FA, Nitschke R, McWilliams NB, Green AA. Cellular DNA content as a predictor of response to chemotherapy in infants with unresectable neuroblastoma. *N Engl J Med* 1984; **311**: 231–5.
4 Schwab M, Alitalo K, Klempnauer KH *et al.* Amplified DNA with limited homology to myc cellular oncogene is shared by human neuroblastoma cell lines and a neuroblastoma tumour. *Nature* 1983; **305**: 245–8.
5 Brodeur GM, Seeger RC, Schwab M, Varmus HE, Bishop JM. Amplification of N-myc in untreated human neuroblastomas correlates with advanced disease stage. *Science* 1984; **224**: 1121–4.
6 Bown N, Cotterill S, Lastowska M *et al.* Gain of chromosome arm 17q and adverse outcome in patients with neuroblastoma. *N Engl J Med* 1999; **340**: 1954–61.
7 Attiyeh EF, London WB, Mosse YP *et al.* Chromosome 1p and 11q deletions and outcome in neuroblastoma. *N Engl J Med* 2005; **353**: 2243–53.
8 Ohira M, Morohashi A, Inuzuka H *et al.* Expression profiling and characterization of 4200 genes cloned from primary neuroblastomas: identification of 305 genes differentially expressed between favorable and unfavorable subsets. *Oncogene* 2003; **22**: 5525–36.
9 Ohira M, Morohashi A, Nakamura Y *et al.* Neuroblastoma oligo-capping cDNA project: toward the understanding of the genesis and biology of neuroblastoma. *Cancer Lett* 2003; **197**: 63–8.
10 Nakagawara A, Arima M, Azar CG, Scavarda NJ, Brodeur GM. Inverse relationship between trk expression and N-myc amplification in human neuroblastomas. *Cancer Res* 1992; **52**: 1364–8.
11 Nakagawara A, Arima-Nakagawara M, Scavarda NJ, Azar CG, Cantor AB, Brodeur GM. Association between high levels of expression of the TRK gene and favorable outcome in human neuroblastoma. *N Engl J Med* 1993; **328**: 847–54.
12 Nakagawara A, Milbrandt J, Muramatsu T *et al.* Differential expression of pleiotrophin and midkine in advanced neuroblastomas. *Cancer Res* 1995; **55**: 1792–7.
13 Tanaka T, Slamon DJ, Shimoda H *et al.* Expression of Ha-ras oncogene products in human neuroblastomas and the significant correlation with a patient's prognosis. *Cancer Res* 1988; **48**: 1030–4.
14 Kawamoto T, Ohira M, Hamano S, Hori T, Nakagawara A. High expression of the novel endothelin-converting enzyme genes, Nbla03145/ECEL1alpha and beta, is associated with favorable prognosis in human neuroblastomas. *Int J Oncol* 2003; **22**: 815–22.
15 Hamano S, Ohira M, Isogai E, Nakada K, Nakagawara A. Identification of novel human neuronal leucine-rich repeat (hNLRR) family genes and inverse association of expression of Nbla10449/hNLRR-1 and Nbla10677/hNLRR-3 with the prognosis of primary neuroblastomas. *Int J Oncol* 2004; **24**: 1457–66.
16 Machida T, Fujita T, Oo ML *et al.* Increased expression of proapoptotic BMCC1, a novel gene with the BNIP2 and Cdc42GAP homology (BCH) domain, is associated with favorable prognosis in human neuroblastomas. *Oncogene* 2006; **25**: 1931–42.
17 Li Y, Ozaki T, Kikuchi H, Yamamoto H, Ohira M, Nakagawara A. A novel HECT-type E3 ubiquitin protein ligase NEDL1 enhances the p53-mediated apoptotic cell death in its catalytic activity-independent manner. *Oncogene* 2008; **27**: 3700–9.
18 Huang S, Laoukili J, Epping MT *et al.* ZNF423 is critically required for retinoic acid-induced differentiation and is a marker of neuroblastoma outcome. *Cancer Cell* 2009; **15**: 328–40.
19 Nakagawara A, Azar CG, Scavarda NJ, Brodeur GM. Expression and function of TRK-B and BDNF in human neuroblastomas. *Mol Cell Biol* 1994; **14**: 759–67.
20 Hiyama E, Hiyama K, Yokoyama T, Matsuura Y, Piatyszek MA, Shay JW. Correlating telomerase activity levels with human neuroblastoma outcomes. *Nat Med* 1995; **1**: 249–55.
21 Hossain MS, Ozaki T, Wang H *et al.* N-MYC promotes cell proliferation through a direct transactivation of neuronal leucine-rich repeat protein-1 (NLRR1) gene in neuroblastoma. *Oncogene* 2008; **27**: 6075–82.
22 Aoyama M, Ozaki T, Inuzuka H *et al.* LMO3 interacts with neuronal transcription factor, HEN2, and acts as an oncogene in neuroblastoma. *Cancer Res* 2005; **65**: 4587–97.
23 Islam A, Kageyama H, Takada N *et al.* High expression of Survivin, mapped to 17q25, is significantly associated with poor prognostic factors and promotes cell survival in human neuroblastoma. *Oncogene* 2000; **19**: 617–23.
24 Godfried MB, Veenstra M, v Sluis P *et al.* The N-myc and c-myc downstream pathways include the chromosome 17q genes nm23-H1 and nm23-H2. *Oncogene* 2002; **21**: 2097–101.
25 Okabe-Kado J, Kasukabe T, Honma Y, Hanada R, Nakagawara A, Kaneko Y. Clinical significance of serum NM23-H1 protein in neuroblastoma. *Cancer Sci* 2005; **96**: 653–60.
26 Saito-Ohara F, Imoto I, Inoue J *et al.* PPM1D is a potential target for 17q gain in neuroblastoma. *Cancer Res* 2003; **63**: 1876–83.
27 Ando K, Ohira M, Ozaki T *et al.* Expression of TSLC1, a candidate tumorsuppressor gene mapped to chromosome 11q23, is downregulated in unfavorable neuroblastoma without promoter hypermethylation. *Int J Cancer* 2008; **123**: 2087–94.
28 Nowacki S, Skowron M, Oberthuer A *et al.* Expression of the tumour suppressor gene CADM1 is associated with favourable outcome and inhibits cell survival in neuroblastoma. *Oncogene* 2008; **27**: 3329–38.
29 Berwanger B, Hartmann O, Bergmann E *et al.* Loss of a FYN-regulated differentiation and growth arrest pathway in advanced stage neuroblastoma. *Cancer Cell* 2002; **2**: 377–86.




doi: 10.1111/j.1349-7006.2010.01681.x

30 Miyake I, Hakomori Y, Shinohara A *et al.* Activation of anaplastic lymphoma kinase is responsible for hyperphosphorylation of ShcC in neuroblastoma cell lines. *Oncogene* 2002; **21**: 5823–34.
31 Miyake I, Ohira M, Nakagawara A, Sakai R. Distinct role of ShcC dockingprotein in the differentiation of neuroblastoma. *Oncogene* 2009; **28**: 662–73.
32 Terui E, Matsunaga T, Yoshida H *et al.* Shc family expression in neuroblastoma: high expression of shcC is associated with a poor prognosis in advanced neuroblastoma. *Clin Cancer Res* 2005; **11**: 3280–7.
33 Boon K, Caron HN, van Asperen R *et al.* N-myc enhances the expression of a large set of genes functioning in ribosome biogenesis and protein synthesis. *EMBO J* 2001; **20**: 1383–93.
34 Alaminos M, Mora J, Cheung NK *et al.* Genome-wide analysis of gene expression associated with MYCN in human neuroblastoma. *Cancer Res* 2003; **63**: 4538–46.
35 Evans AE, D'Angio GJ, Randolph J. A proposed staging for children with neuroblastoma. Children's cancer study group A. *Cancer* 1971; **27**: 374–8.
36 London WB, Castleberry RP, Matthay KK *et al.* Evidence for an age cutoff greater than 365 days for neuroblastoma risk group stratification in the Children's Oncology Group. *J Clin Oncol* 2005; **23**: 6459–65.
37 Brodeur GM, Pritchard J, Berthold F *et al.* Revisions of the international criteria for neuroblastoma diagnosis, staging, and response to treatment. *J Clin Oncol* 1993; **11**: 1466–77.
38 Shimada H, Ambros IM, Dehner LP *et al.* The International Neuroblastoma Pathology Classification the Shimada system. *Cancer* 1999; **86**: 364–72.
39 van't Veer LJ, Dai H, van de Vijver MJ *et al.* Gene expression profiling predicts clinical outcome of breast cancer. *Nature* 2002; **415**: 530–6.
40 Wei JS, Greer BT, Westermann F *et al.* Prediction of clinical outcome using gene expression profiling and artificial neural networks for patients with neuroblastoma. *Cancer Res* 2004; **64**: 6883–91.
41 Ohira M, Oba S, Nakamura Y *et al.* Expression profiling using a tumor-specific cDNA microarray predicts the prognosis of intermediate risk neuroblastomas. *Cancer Cell* 2005; **7**: 337–50.
42 Oberthuer A, Berthold F, Warnat P *et al.* Customized oligonucleotide microarray gene expression-based classification of neuroblastoma patients outperforms current clinical risk stratification. *J Clin Oncol* 2006; **24**: 5070–8.
43 Asgharzadeh S, Pique-Regi R, Sposto R *et al.* Prognostic significance of gene expression profiles of metastatic neuroblastomas lacking MYCN gene amplification. *J Natl Cancer Inst* 2006; **98**: 1193–203.
44 Schramm A, Vandesompele J, Schulte JH *et al.* Translating expression profiling into a clinically feasible test to predict neuroblastoma outcome. *Clin Cancer Res* 2007; **13**: 1459–65.
45 Chen QR, Song YK, Wei JS *et al.* An integrated cross-platform prognosis study on neuroblastoma patients. *Genomics* 2008; **92**: 195–203.
46 Vermeulen J, De Preter K, Naranjo A *et al.* Predicting outcomes for children with neuroblastoma using a multigene-expression signature: a retrospective SIOPEN/COG/GPOH study. *Lancet Oncol* 2009; **10**: 663–71.
47 Mosse YP, Greshock J, Margolin A *et al.* High-resolution detection and mapping of genomic DNA alterations in neuroblastoma. *Genes Chromosomes Cancer* 2005; **43**: 390–403.
48 Wang Q, Diskin S, Rappaport E *et al.* Integrative genomics identifies distinct molecular classes of neuroblastoma and shows that multiple genes are targeted by regional alterations in DNA copy number. *Cancer Res* 2006; **66**: 6050–62.
49 Tomioka N, Oba S, Ohira M *et al.* Novel risk stratification of patients with neuroblastoma by genomic signature, which is independent of molecular signature. *Oncogene* 2008; **27**: 441–9.
50 Janoueix-Lerosey I, Schleiermacher G, Michels E *et al.* Overall genomic pattern is a predictor of outcome in neuroblastoma. *J Clin Oncol* 2009; **27**: 1026–33.
51 Mosse YP, Laudenslager M, Longo L *et al.* Identification of ALK as a major familial neuroblastoma predisposition gene. *Nature* 2008; **455**: 930–5.
52 Chen Y, Takita J, Choi YL *et al.* Oncogenic mutations of ALK kinase in neuroblastoma. *Nature* 2008; **455**: 971–4.
53 Janoueix-Lerosey I, Lequin D, Brugieres L *et al.* Somatic and germline activating mutations of the ALK kinase receptor in neuroblastoma. *Nature* 2008; **455**: 967–70.
54 George RE, Sanda T, Hanna M *et al.* Activating mutations in ALK provide a therapeutic target in neuroblastoma. *Nature* 2008; **455**: 975–8.
55 Osajima-Hakomori Y, Miyake I, Ohira M, Nakagawara A, Nakagawa A, Sakai R. Biological role of anaplastic lymphoma kinase in neuroblastoma. *Am J Pathol* 2005; **167**: 213–22.
56 Rongshi L, Morris SW. Development of anaplastic lymphoma kinase (ALK) small-molecule inhibitors for cancer therapy. *Med Res Rev* 2008; **28**: 372–412.
57 Amiel J, Laudier B, Attie-Bitach T *et al.* Polyalanine expansion and frameshift mutations of the paired-like homeobox gene PHOX2B in congenital central hypoventilation syndrome. *Nat Genet* 2003; **33**: 459–61.
58 Mosse YP, Laudenslager M, Khazi D *et al.* Germline PHOX2B mutation in hereditary neuroblastoma. *Am J Hum Genet* 2004; **75**: 727–30.
59 Trochet D, Bourdeaut F, Janoueix-Lerosey I *et al.* Germline mutations of the paired-like homeobox 2B PHOX2B; gene in neuroblastoma. *Am J Hum Genet* 2004; **74**: 761–4.
60 Maris JM, Mosse YP, Bradfield JP *et al.* Chromosome 6p22 locus associated with clinically aggressive neuroblastoma. *N Engl J Med* 2008; **358**: 2585–93.
61 Capasso M, Devoto M, Hou C *et al.* Common variations in BARD1 influence susceptibility to high-risk neuroblastoma. *Nat Genet* 2009; **41**: 718–23.
62 Diskin SJ, Hou C, Glessner JT *et al.* CNV Copy number variation at 1q21.1 associated with neuroblastoma. *Nature* 2009; **459**: 987–91.
63 Yang Q, Kiernan CM, Tian Y *et al.* Methylation of CASP8, DCR2, and HIN-1 in neuroblastoma is associated with poor outcome. *Clin Cancer Res* 2007; **13**: 3191–7.
64 Abe M, Ohira M, Kaneda A *et al.* CpG island methylator phenotype is a strong determinant of poor prognosis in neuroblastomas. *Cancer Res* 2005; **65**: 828–34.
65 Abe M, Westermann F, Nakagawara A, Takato T, Schwab M, Ushijima T. Marked and independent prognostic significance of the CpG island methylator phenotype in neuroblastomas. *Cancer Lett* 2007; **247**: 253–8.
66 Abe M, Watanabe N, McDonell N *et al.* Identification of genes targeted by CpG island methylator phenotype in neuroblastomas, and their possible integrative involvement in poor prognosis. *Oncology* 2008; **74**: 50–60.
67 Yagyu S, Gotoh T, Iehara T *et al.* Circulating methylated-DCR2 gene in serum as an indicator of prognosis and therapeutic efficacy in patients with MYCN nonamplified neuroblastoma. *Clin Cancer Res* 2008; **14**: 7011–19.
68 Misawa A, Tanaka S, Yagyu S *et al.* RASSF1A hypermethylation in pretreatment serum DNA of neuroblastoma patients: a prognostic marker. *Br J Cancer* 2009; **100**: 399–404.
69 Mattick JS, Makunin IV. Non-coding RNA. *Hum Mol Genet* 2006; **15**: R17–19.
70 Prasanth KV, Spector DL. Eukaryotic regulatory RNAs: an answer to the 'genome complexity' conundrum. *Genes Dev* 2007; **21**: 11–42.
71 Welch C, Chen Y, Stallings RL. MicroRNA-34a functions as a potential tumor suppressor by inducing apoptosis in neuroblastoma cells. *Oncogene* 2007; **26**: 5017–22.
72 Cole KA, Attiyeh EF, Mosse YP *et al.* A functional screen identifies miR-34a as a candidate neuroblastoma tumor suppressor gene. *Mol Cancer Res* 2008; **6**: 735–42.
73 Wei JS, Song YK, Durinck S *et al.* The MYCN oncogene is a direct target of miR-34a. *Oncogene* 2008; **27**: 5204–13.
74 Fontana L, Fiori ME, Albini S *et al.* Antagomir-17-5p abolishes the growth of therapy-resistant neuroblastoma through p21 and BIM. *PLoS ONE* 2008; **3**: e2236.
75 Ma L, Young J, Prabhala H *et al.* miR-9, a MYC/MYCN-activated microRNA, regulates E-cadherin and cancer metastasis. *Nat Cell Biol* 2010; **12**: 247–58.
76 Chen Y, Stallings RL. Differential patterns of microRNA expression in neuroblastoma are correlated with prognosis, differentiation, and apoptosis. *Cancer Res* 2007; **67**: 976–83.
77 Schulte JH, Horn S, Otto T *et al.* MYCN regulates oncogenic microRNAs in neuroblastoma. *Int J Cancer* 2008; **122**: 699–704.
78 Buckley PG, Alcock L, Bryan K *et al.* Chromosomal and microRNA expression patterns reveal biologically distinct subgroups of 11q-neuroblastoma. *Clin Cancer Res* 2010; **16**: 2971–8.
79 Bray I, Bryan K, Prenter S *et al.* Widespread dysregulation of miRNAs by MYCN amplification and chromosomal imbalances in neuroblastoma: association of miRNA expression with survival. *PLoS ONE* 2009; **4**: e7850.
80 Yu M, Ohira M, Li Y *et al.* High expression of ncRAN, a novel non-coding RNA mapped to chromosome 17q25.1, is associated with poor prognosis in neuroblastoma. *Int J Oncol* 2009; **34**: 931–8.

# Murine induced pluripotent stem cells can be derived from and differentiate into natural killer T cells

Hiroshi Watarai,[1,2] Shin-ichiro Fujii,[1] Daisuke Yamada,[1,2] Andrei Rybouchkin,[1] Sakura Sakata,[1] Yuko Nagata,[1] Midori Iida-Kobayashi,[1,2] Etsuko Sekine-Kondo,[1] Kanako Shimizu,[1] Yohei Shozaki,[1] Jafar Sharif,[1] Masashi Matsuda,[1] Shinobu Mochiduki,[1] Takanori Hasegawa,[1] Genta Kitahara,[1] Takaho A. Endo,[3] Tetsuro Toyoda,[3] Osamu Ohara,[1] Ken-ichi Harigaya,[4] Haruhiko Koseki,[1,2] and Masaru Taniguchi[1]

[1]RIKEN Research Center for Allergy and Immunology, Yokohama, Japan. [2]Core Research for Evolutional Science and Technology (CREST), Japan Science and Technology Corporation (JST), Tokyo, Japan. [3]RIKEN BASE, Yokohama, Japan. [4]Department of Pathology, Graduate School of Medicine, Chiba University, Chiba, Japan.

**NKT cells demonstrate antitumor activity when activated to produce Th1 cytokines by DCs loaded with α-galactosylceramide, the prototypic NKT cell–activating glycolipid antigen. However, most patients do not have sufficient numbers of NKT cells to induce an effective immune response in this context, indicating a need for a source of NKT cells that could be used to supplement the endogenous cell population. Induced pluripotent stem cells (iPSCs) hold tremendous potential for cell-replacement therapy, but whether it is possible to generate functionally competent NKT cells from iPSCs has not been rigorously assessed. In this study, we successfully derived iPSCs both from embryonic fibroblasts from mice harboring functional NKT cell–specific rearranged T cell receptor loci in the germline and from splenic NKT cells from WT adult mice. These iPSCs could be differentiated into NKT cells in vitro and secreted large amounts of the Th1 cytokine IFN-γ. Importantly, iPSC-derived NKT cells recapitulated the known adjuvant effects of natural NKT cells and suppressed tumor growth in vivo. These studies demonstrate the feasibility of expanding functionally competent NKT cells via an iPSC phase, an approach that may be adapted for NKT cell–targeted therapy in humans.**

## Introduction

NKT cells are characterized by their expression of an invariant TCR α chain encoded by *Vα14-Jα18* in mice (1) and by *Vα24-Jα18* in humans (2, 3). NKT cells recognize glycolipid antigens and can be efficiently activated through recognition of α-galactosylceramide (α-GalCer) in the context of CD1d, a monomorphic MHC class I–like molecule (4). Although activated NKT cells produce both Th1 and Th2 cytokines, they mediate strong adjuvant activity essential for protective responses against tumors (5–7) and pathogens through their production of Th1 cytokines.

Based on these observations, α-GalCer can be used as a drug for clinical applications. Several clinical trials with injection of $5 \times 10^6$ α-GalCer–pulsed DCs have been carried out in patients with cancer, including colon cancer (8, 9), multiple myeloma, anal cancer, and renal cell cancer (10). Although no clear tumor reduction was detected, tumor markers were significantly decreased.

A more extensive phase I/IIa clinical trial of α-GalCer–loaded DC therapy (total $4 \times 10^9$ cells per person in 4 consecutive injections at 1 week intervals) for advanced lung cancer patients (stages IIIB, IV, and recurrent) was launched. Encouragingly, this trial validated the antitumor effects of NKT cells in humans, since 60% of 17 enrolled patients with only a primary treatment showed a prolonged median survival time (MST) of 31.9 months without tumor progression and metastasis compared with the MST of 4.6 months under the best supportive care (11). However, despite its clear antitumor activity, two-thirds of patients were not eligible for NKT cell–targeted therapy because they no longer had sufficient NKT cells (less than 10 cells/ml of blood) (12). These observations underscore the urgent need to establish an efficient method to supplement NKT cells.

Results from our previous study, in which we used embryonic stem cells (ESC) derived from NKT cell–cloned mice (hereafter called the NKT mouse) established by nuclear transfer from C57BL/6 (B6) hepatic NKT cells, had already suggested that these cells could give rise to NKT cells both in vivo and in vitro (13). Since induced pluripotent stem cells (iPSCs) and ESCs are functionally equivalent in many respects, these observations suggested the feasibility of the clinical potential of iPSCs for NKT cell–targeted adjuvant therapy (14–16). Moreover, it is important to mention that iPSCs rather than ESCs are more feasible in the clinical setting because embryos or donor oocytes are not required for generation of iPSCs. In addition, iPSCs are fully syngeneic, while ESCs, even if introduced with patient cell nucleus, carrying oocyte-derived mitochondrial maternal antigens may cause problems in generating allogeneic immune responses. The present study has been designed to examine the feasibility of ex vivo generation of functionally competent NKT cells from iPSCs. Here, we have addressed 2 specific issues: (a) generation of iPSCs from mature NKT cells and their in vitro generation of functional NKT cells, and (b) investigation of the adjuvant activity of iPSC-derived NKT cells transferred in vivo and their clinical potential in a mouse model.

**Authorship note:** Hiroshi Watarai and Shin-ichiro Fujii contributed equally to this work.

**Conflict of interest:** The authors have declared that no conflict of interest exists.

**Citation for this article:** *J Clin Invest.* 2010;120(7):2610–2618. doi:10.1172/JCI42027.

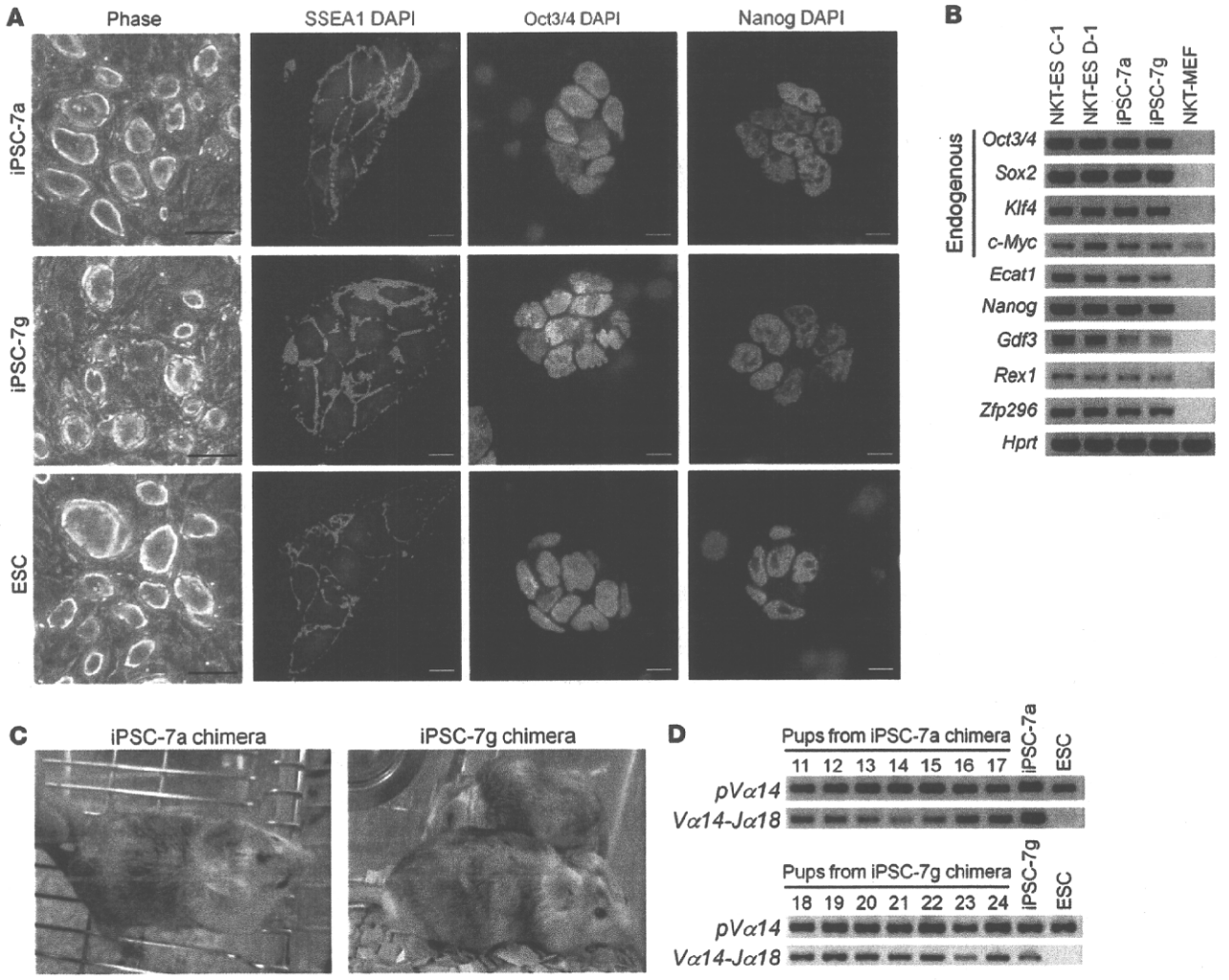


**Figure 1**

Generation of iPSCs harboring NKT cell–specific rearranged T cell receptor loci. (**A**) Colony shape and the expression of stage-specific embryo antigen 1 (SSEA1), Octamer-binding protein 3/4 (Oct3/4), and Nanog in the iPSC-7a and iPSC-7g cells. ESCs are shown as a reference. Scale bars: 100 μm (phase); 10 μm (immunofluorescence). (**B**) Expression of ESC marker genes in iPSC-7a and iPSC-7g cells. Results for RT-PCR analyses are shown. NKT-ES C-1 and NKT-ES D-1 were used as positive controls, and NKT-MEF was used as a negative control. (**C**) External views of chimeras generated by injecting iPSC-7a and iPSC-7g cells into BALB/c blastocysts. (**D**) Transmission of the rearranged *Tcra* chain locus to the offspring of chimeras, which is characteristic of iPSC-7a (upper panel) and iPSC-7g cells (lower panel).

## Results

*Generation of iPSCs harboring NKT cell–specific rearranged T cell receptor loci.* Mouse embryonic fibroblasts obtained from the NKT mice (NKT-MEF) that had been established from ESCs generated by NKT cell nuclear transfer (NKT-ES) (13) were reprogrammed to generate iPSCs using a conventional protocol with retroviral vectors (14). Eight ESC-like colonies were selected and expanded in ES medium. We found that most of the lines stably exhibited ESC-like morphology and selected lines, iPSC-7a and iPSC-7g, for further analysis to verify that they were indeed iPSCs. We analyzed their expression of molecular markers that define iPSCs and determined the degree of reprogramming and their ability to generate teratomas and chimeras.

Immunofluorescence analysis revealed that the expression of SSEA1, Oct3/4, and Nanog in both the iPSC-7a and iPSC-7g lines was similar to that in the control ESCs (Figure 1A). We also detected the expression of endogenous *Oct3/4*, *Sox2*, *Klf4*, *Nanog*, *Ecat1*, *Gdf3*, *Rex1*, and *Zfp296* by RT-PCR analysis (Figure 1B). Consistent with the reactivated expression of Oct3/4 and Nanog in the iPSC-7a and iPSC-7g cells, DNA methylation patterns at these gene loci were similar to ESCs and significantly reduced in comparison with the parental NKT-MEF (Supplemental Figure 1; supplemental material available online with this article; doi:10.1172/JCI42027DS1).

We went on to compare the gene expression profiles of the iPSC-7a and iPSC-7g cells against NKT-ES and NKT-MEF. The genome-wide expression profile of the iPSC-7a cells showed a much higher correlation coefficient to NKT-ES C-1 than to the parental NKT-MEF (Supplemental Figure 2A). Cluster analysis placed the iPSC-7a and iPSC-7g cells in the NKT-ES (C-1 and D-1) or ESCs but not the NKT-MEF, iPSC-derived NKT cells (7a-NKT and 7g-NKT) nor

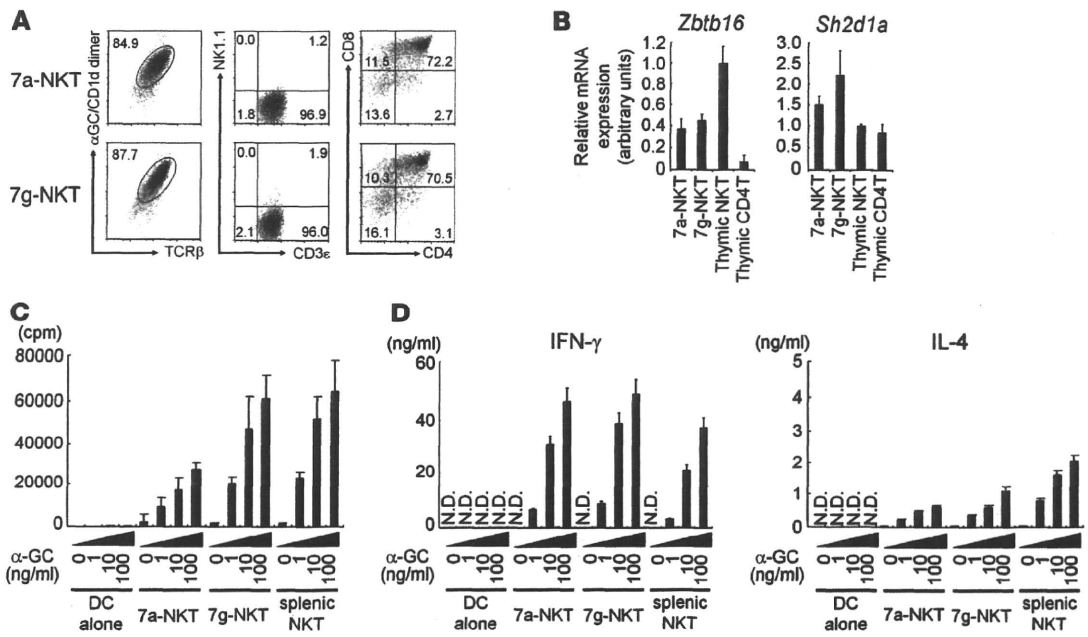


**Figure 2**

In vitro generation of NKT cells from iPSCs in the 25-day culture system. (**A**) Expression of cell surface markers on iPSC-derived NKT cells (7a-NKT and 7g-NKT). 7a-NKT and 7g-NKT cells generated in vitro were gated as the α-GalCer/CD1d dimer$^+$TCR-β$^+$ population and further analyzed for the expression of the indicated markers, NK1.1 versus CD3ε and CD4 versus CD8. Numbers show percentage of each gate. (**B**) Quantitative PCR analysis. Indicated genes in iPSC-derived NKT cells and FACS-sorted thymic NKT and CD4 T cells were analyzed for mRNA levels by quantitative real-time PCR ($2 \times 10^3$ cells/sample). (**C** and **D**) Proliferative response (**C**) and cytokine production (**D**) of iPSC-derived NKT cells upon stimulation with α-GalCer. The 7a-NKT, 7g-NKT, or WT splenic NKT cells ($10^6$/ml) were cocultured with bone marrow–derived DCs ($10^5$/ml) in the presence of the indicated dose of α-GalCer (0, 1, 10, 100 ng/ml). Mean ± SD of triplicate wells is shown. One representative experiment of 3 is shown.

splenic NKT cell (NKT 1 and NKT 2) cluster (Supplemental Figure 2, B and C). Therefore, the iPSC-7a and iPSC-7g cells were sufficiently reprogrammed. Furthermore, we tested the ability of these cells to form teratomas in nude mice and produce germline chimeras upon blastocyst injection. Both iPSC-7a and iPSC-7g cells formed teratomas with 3 germ layers upon s.c. injection into nude mice (D. Yamada and H. Koseki, unpublished observations), and when injected into BALB/c blastocysts, they generated 7 and 3 coat color chimeras, respectively (Figure 1C). The male chimeras tested were found to be germline chimeras that transmitted the rearranged *Tcra* loci to their offspring (Figure 1D). We thus concluded the iPSC-7a and iPSC-7g lines satisfied all the known criteria for iPSCs.

*In vitro generation of NKT cells from iPSCs in the 20-day culture system.* We first attempted to investigate the potential of NKT cell development from iPSC-7a and iPSC-7g in the 20-day culture system used for analysis of ESCs described previously (Supplemental Figure 3A) (13). Similar to ESC-derived NKT cells, iPSC-derived NKT cells mainly produced IL-4 on OP9/Dll-1 culture for 20 days, while mainly producing IFN-γ in the switching culture on OP9/control starting at day 14 (Supplemental Figure 3B), indicating that iPSCs are potentially the same as ESCs. Moreover, the yield of NKT cells from the Notch-dependent conditions was $3 \times 10^6$ from $1 \times 10^5$ iPSCs (30 times), while those from Notch-independent conditions were only $3 \times 10^5$ (3 times). Thus, the culture conditions with or without Notch signaling reflected the proliferation activity of iPSC-derived NKT cells such as ESC-derived NKT cells in vitro (Supplemental Figure 3C).

*The 25-day culture system efficient for generation of iPSC-derived NKT cells producing large amounts of IFN-γ.* It is important to obtain a high yield of NKT cells with the desired function for the establishment of NKT cell therapy. For this purpose, we attempted to develop a new 25-day culture system efficiently to generate functional NKT cells from the iPSC-7a and iPSC-7g cells in vitro. Since proliferative activity is totally depend on Notch signaling (Supplemental Figure 3D), iPSCs were cocultured on OP9/Dll-1 in the presence of various cytokine combinations to manipulate NKT cell function (Supplemental Figure 4A). The addition of IL-15 at culture day 20 for 5 days suppressed the proliferative function of NKT cells (Supplemental Figure 4B), while IL-2 promoted NKT cell expansion but suppressed IFN-γ production upon stimulation with α-GalCer (Supplemental Figure 4B). In contrast with the above cytokines, the addition of both IL-7 and Flt-3 ligand (Flt3L) at the culture day 20 for 5 days yielded the highest number of NKT cells and also the highest amounts of IFN-γ production (Supplemental Figure 4B), which are equivalent to those by splenic NKT cells (see Figure 2D). Under these conditions, $1 \times 10^5$ iPSCs gave rise to $3 \times 10^7$ iPSC-derived NKT cells at culture day 25 (Supplemental Figure 4C) that expressed TCR-β on their surface and bound α-GalCer–loaded soluble CD1d dimer, which are specifically recognized by the NKT-specific TCR (Figure 2A). The iPSC-derived NKT cells (7a-NKT and 7g-NKT) did not express NK1.1 (Figure 2A). Moreover, a significant fraction of the 7a-NKT and 7g-NKT cells were doubly positive for CD4 and CD8 (Figure 2A). Therefore, the iPSC-derived NKT cells generated in this 25-day culture

system were more similar to immature $CD4^+CD8^+$ (double-positive [DP]) thymocytes than to mature liver NKT cells. Moreover, they were $CD24^{hi}$, $CD44^{lo/int}$, $CD62L^{hi}$, $CD69^+$, $CD122^{lo/-}$, and $NKG2D^-$, which phenotypically resemble the earliest thymic NKT cells, so-called stage 0 NKT cells (Supplemental Figure 5). The iPSC-derived NKT cells expressed significant levels of *Zbtb16* (also known as PLZF) (17, 18) and also *Sh2d1a* (also known as SAP) (19, 20) compared with those of thymic CD4 T cells, indicating that iPSC-derived cells are phenotypically immature and likely to be typical NKT cells, but not conventional T cells (Figure 2B).

To further investigate functional activity of iPSC-derived NKT cells, proliferative responses and cytokine production were investigated upon stimulation with α-GalCer–pulsed DCs (Figure 2, C and D). The iPSC-derived NKT cells from both iPSC-7a and iPSC-7g proliferated similarly to splenic NKT cells (Figure 2C). The cytokines, such as IFN-γ, IL-4, IL-5, IL-10, and IL-13, were also produced by iPSC-derived NKT cells at levels similar to those of splenic NKT cells (Figure 2D and Supplemental Figure 6). Taken together, these observations indicated that the iPSC-derived NKT cells possess functional properties similar to those of NKT cells. It is also important to mention that, as opposed to the 20-day culture system used for iPSC-derived (Supplemental Figure 3) or ES-derived NKT cell development (13), the 25-day culture system yielded 10 times the number of NKT cells and produced 5 times the amount of IFN-γ (Figure 2 and Supplemental Figure 4).

*Adjuvant activity of iPSC-derived NKT cells.* We then addressed whether iPSC-derived NKT cells (7a-NKT or 7g-NKT) can exert adjuvant activity in vivo in mice. We and others have previously developed an experimental model to evaluate the adjuvant activity of activated NKT cells (21–24). In this model, we observed significant enhancement of antigen-specific CD8 T cell priming by coadministration of OVA-loaded dying spleen cells from $TAP^{-/-}$ mice ($2 \times 10^7$/mouse) with 2 μg α-GalCer (TOG) in an NKT cell–dependent manner (Supplemental Figure 7) (23, 24). We first determined whether iPSC-derived NKT cells could repopulate in the recipient tissues after adoptive transfer into $J\alpha18^{-/-}$ mice, which lack endogenous NKT cells. A considerable number of the 7a-NKT and 7g-NKT cells were detectable in the liver of $J\alpha18^{-/-}$ mice 1 and 2 weeks after the transfer (Figure 3A). These cell numbers are almost similar to those of WT mature liver NKT cells transferred into $J\alpha18^{-/-}$ mice. Interestingly, 7a-NKT and 7g-NKT cells detected in the liver were $CD24^{lo}$, $CD44^{hi}$, $CD62L^{lo}$, $CD69^+$, $CD122^+$, and $NKG2D^+$, phenotypically similar to mature liver NKT cells in WT mice (Supplemental Figure 8), indicating the maturation of their phenotypes in vivo. To test the ability of IFN-γ production from iPSC-derived NKT cells upon antigen stimulation, the mice that received the 7a-NKT or 7g-NKT cells were injected with α-GalCer i.v. α-GalCer administration led to the significant expansion (0.3%–0.4% [Figure 3A] vs. 4.9%–5.7% [Figure 3B]) of 7a-NKT and 7g-NKT cells with downmodulated TCR-β expression (Figure 3B vs. Figure 3A) and significant IFN-γ production (Figure 3B), indicating the in vivo activation of iPSC-derived NKT cells. Moreover, we observed in vivo bystander adjuvant effects on $NK1.1^+TCR\text{-}\beta^-$ cells after activation of iPSC-derived NKT cells in terms of their significant IFN-γ production (Figure 3C).

We further investigated the bystander adjuvant activity by the iPSC-derived NKT cells on CD8 T cells in vivo, in which the mice transferred with the 7a-NKT or 7g-NKT cells were immunized with TOG and examined for the extent of induction of OVA-specific, IFN-γ–producing CD8 T cells. We indeed observed a significant increase in the number of these CD8 T cells (10–50 times increases over the control group) (Figure 3, D and E). Thus, the iPSC-derived NKT cells were shown to function as a cellular adjuvant for both innate and adaptive immune responses.

We next adoptively transferred the 7a-NKT or 7g-NKT cells into $J\alpha18^{-/-}$ mice to test for their acquisition of antigen-specific antitumor activity. Seven days after the adoptive transfer, mice were primed with TOG, challenged with EL4, a B6-derived thymoma line, or with the OVA-expressing EL4 subline EG7 ($2 \times 10^5$ cells injected s.c.), and then observed for tumor growth. In this model, we observed strong antitumor activity against EG7 but not EL4 in TOG-immunized B6 mice but not in $J\alpha18^{-/-}$ mice (Figure 3F). The growth of EG7 tumor cells in $J\alpha18^{-/-}$ mice was significantly suppressed by adoptive transfer of the 7a-NKT or 7g-NKT cells, whereas the growth of EL4 was not. These results indicate that the iPSC-derived NKT cells can enhance the generation of functionally sufficient numbers of antigen-specific CD8 T cells to exert antitumor immunity. Therefore, the iPSC-derived NKT cells are functionally competent to mediate adjuvant activity in vivo.

*Generation of iPSC from splenic NKT cells.* We finally confirmed splenic NKT cells also could be reprogrammed into iPSCs. NKT cells ($1 \times 10^6$) were isolated from normal B6 splenocytes and then activated by anti-CD3/CD28 magnetic beads together with IL-12 (10 ng/ml) and IL-2 (10 ng/ml) for 1 week, followed by reprogramming according to the conventional protocol (14). From 2 experiments, we established at least 3 independent iPSC-like lines. After confirming that the 14k cell line (iPSC-14k) was NKT cell–derived, based on the nucleotide and deduced amino acid sequences of the CDR3 junctional regions of the *Tcra* and *Tcrb* loci (Figure 4A), we focused on this line to determine whether it is an authentic iPSC. Immunofluorescent analysis revealed the expression of SSEA1, Oct3/4, and Nanog in the iPSC-14k cells (Figure 4B) and the expression of endogenous *Oct3/4*, *Sox2*, *Klf4*, *Nanog*, *Ecat1*, *Gdf3*, *Rex1*, and *Zfp296* mRNA could be detected by RT-PCR (Figure 4C). Genome-wide gene expression profiles of the iPSC-14k cells showed a higher correlation coefficient to ESCs or iPSCs, such as NKT-ES C-1 and iPSC-7a or iPSC-7g, than to splenic NKT cells (Figure 4D and Supplemental Figure 9A). Therefore, the iPSC-14k cells were shown to be adequately reprogrammed. We went on to test the ability of these cells to form teratomas and chimeras as described above. Teratomas with 3 germ layers were generated from the iPSC-14k cells upon s.c. injection into nude mice (Supplemental Figure 9B). Three coat color chimeras were generated upon injection into BALB/c blastocysts, and one of them was a germline chimera (Figure 4E). Taken together, the iPSC-14k cells were confirmed to be an authentic iPSC line.

We further examined the redifferentiation potential of the iPSC-14k cells into splenic NKT cells in vitro in the 25-day culture system. In the culture system, the iPSC-14k cells ($1 \times 10^5$) gave rise to $3 \times 10^7$ α-GalCer/CD1d dimer$^+$TCR-β$^+$ cells, equivalent to the potential of iPSC-7a or iPSC-7g cells. The induced NKT cells were mostly immature $CD4^+CD8^+$ phenotypes (Figure 4F) with $CD24^{hi}$, $CD44^{lo}$, $CD62L^{hi}$, $CD122^{lo}$, $CD69^{lo}$, and $NKG2D^-$ (Supplemental Figure 5), and of note, approximately 30% of them expressed NK1.1 (Figure 4F). α-GalCer/CD1d dimer$^+$TCR-β$^+$ cells derived from the iPSC-14k also exhibited a significant proliferative response and production of IFN-γ and IL-4 upon antigenic stimuli (Figure 4G). Therefore, the iPSC-14k–derived α-GalCer/CD1d dimer$^+$TCR-β$^+$ cells represent NKT cells. However, since some of the cells express NK1.1, their developmental stage may be slightly more advanced compared with those derived from the iPSC-7a or iPSC-7g cells. It is interesting

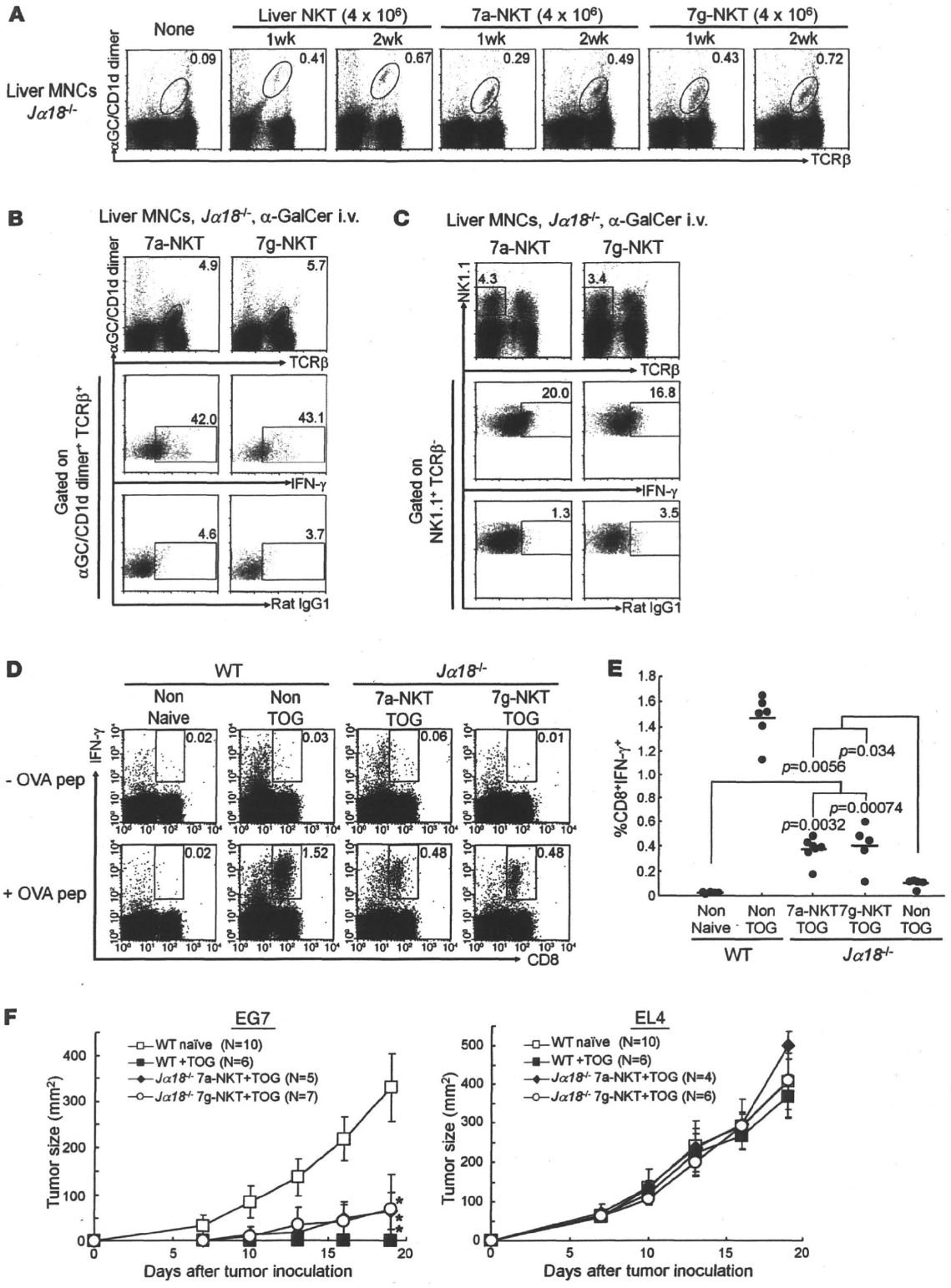
A
None
Liver NKT (4 x 10⁶)
7a-NKT (4 x 10⁶)
7g-NKT (4 x 10⁶)
1wk
2wk
Liver MNCs
Jα18⁻/⁻
αGC/CD1d dimer
TCRβ
0.09
0.41
0.67
0.29
0.49
0.43
0.72
B
Liver MNCs, Jα18⁻/⁻, α-GalCer i.v.
7a-NKT
7g-NKT
Gated on αGC/CD1d dimer⁺ TCRβ⁺
IFN-γ
Rat IgG1
4.9
5.7
42.0
43.1
4.6
3.7
C
Liver MNCs, Jα18⁻/⁻, α-GalCer i.v.
NK1.1
Gated on NK1.1⁺ TCRβ⁻
4.3
3.4
20.0
16.8
1.3
3.5
D
WT
Jα18⁻/⁻
Non Naive
Non TOG
7a-NKT TOG
7g-NKT TOG
- OVA pep
+ OVA pep
CD8
0.02
0.03
0.06
0.01
0.02
1.52
0.48
0.48
E
%CD8⁺IFN-γ⁺
p=0.034
p=0.0056
p=0.00074
p=0.0032
Non Naive
Non TOG
7a-NKT TOG
7g-NKT TOG
Non TOG
WT
Jα18⁻/⁻
F
EG7
EL4
WT naïve (N=10)
WT +TOG (N=6)
Jα18⁻/⁻ 7a-NKT+TOG (N=5)
Jα18⁻/⁻ 7g-NKT+TOG (N=7)
Jα18⁻/⁻ 7a-NKT+TOG (N=4)
Jα18⁻/⁻ 7g-NKT+TOG (N=6)
Tumor size (mm²)
Days after tumor inoculation

**Figure 3**
Adjuvant activity of iPSC-derived NKT cells on antitumor responses in vivo. (**A**) FACS analysis of liver MNCs in $J\alpha18^{-/-}$ mice at indicated time points after adoptive transfer of liver NKT, 7a-NKT, or 7g-NKT cells ($4 \times 10^6$ cell/mouse). (**B** and **C**) In vivo expansion and IFN-γ production of 7a-NKT and 7g-NKT cells (**B**) and their bystander effects on NK cells (**C**). The $J\alpha18^{-/-}$ mice that received iPSC-derived NKT cells were primed i.v. with α-GalCer (2 μg). The indicated cells in liver MNCs in **B** and **C** were investigated for their intracellular IFN-γ production by FACS using anti–IFN-γ compared with rat IgG1. (**D–F**) iPSC-derived NKT cell–mediated bystander adjuvant activity on CD8 T cells (**D** and **E**) and antitumor responses (**F**) based on the experimental procedure shown in Supplemental Figure 7. (**D**) IFN-γ production by CD8 T cells upon restimulation with $OVA_{257-264}$ peptide in vitro. Representative data from 3 experiments are shown. Numbers show percentage of each gate. (**E**) Summary and statistical analysis for the results shown in **D**. The frequency of OVA-specific, IFN-γ–producing CD8 T cells is summarized as percentage of total lymphocytes in the spleen. *P* values indicate differences between each group. (**F**) Adjuvant activity of 7a-NKT and 7g-NKT cells on antitumor responses. Mice were challenged with $2 \times 10^5$ EL4- or OVA-expressing EL4 (EG7) cells s.c. Tumor size in each group was measured at the indicated time points. Mean ± SD from 2 independent experiments is shown. $^*P < 0.01$, differences between WT naive and other groups in EG7-injected mice.

that the ability of iPSC-14k–derived NKT cells to proliferate and to produce IFN-γ was similar to that of iPS-7a–derived NKT cells or splenic NKT cells in the 25-day culture (Figure 2), while no significant responses were obtained by iPSC-14k–derived NKT cells generated in the 20-day culture system (Figure 4G), indicating that the functions of iPSC-derived NKT cells are largely dependent on the duration of the culture in vitro and that at least the 25-day culture period is required to obtain functional iPSC-derived NKT cells.

## Discussion

Although several attempts have been made to generate iPSCs from mature B or T lymphocyte cells by the introduction of *Oct3/4*, *Sox2*, *Klf4*, and *c-Myc*, the efficiency is very low (25). Recently, B- or T-derived iPSCs have efficiently been generated by gene modulation of the myeloid transcription factor CCAAT/enhancer-binding protein-α (C/EBPα) or Pax5 for B cells (26), or of the p53/p21 pathway for T cells (27). However, efforts to regenerate functional B or T lymphocytes from these lymphocyte-derived iPSCs have remained unsuccessful. In the present studies, we have successfully demonstrated for what we believe is the first time the generation of functional NKT cells in vitro from splenic NKT cell–derived iPSCs and also the clinical potential of iPSC-derived NKT cells to control the growth of a syngeneic tumor through their adjuvant activity. Given the promise of patient-specific therapy, it might be prudent to consider the establishment of cell banks of NKT cell–derived iPSCs. Since the functions and antigen specificity of NKT cells are highly conserved between mice and humans, this study has opened up an alternative pathway to realize the potential of NKT cell–targeted therapy in cancer patients. Moreover, NKT cells play multiple roles in modulation of immune responses, such as in antiviral immunity and rejection of transplanted tissues (1, 4). Therefore, therapeutic applications of iPSC-derived NKT cells through their adjuvant activity could be extended to other serious diseases involving immune mechanisms.

Furthermore, this and our previous studies have suggested that derivation of NKT cells from iPSCs does not depend on the cellular origin of the iPSCs but likely on their intrinsic ability to express the invariant TCR that is specific for NKT cells. If this interpretation is correct, it would imply that iPSCs and ESCs could be induced to differentiate into the NKT cell lineage once the appropriate rearranged *Tcr* genes were introduced, either by homologous recombination or simple transfection. Since this approach should be more generally available than the more complex procedure of generating iPSCs from NKT cells by retrovirus-mediated reprogramming, we are currently addressing this possibility in mice.

During the course of this study, we found some subtle differences among iPSC-derived NKT cell lines in their phenotypes and in their ability to proliferate or to produce cytokines (Figure 2 and Supplemental Figure 6). Such functional heterogeneity that is manifested upon differentiation has previously been reported for human ESCs (28). However, in general, there is no significant difference in their phenotypes (Supplemental Figures 5 and 8). The phenotypic changes are largely dependent on culture conditions. In the 20-day culture system, iPSCs cultured on OP9/Dll-1 give rise to NKT cells bearing immature phenotypes similar to $CD4^+CD8^+$ DP thymocytes in vitro as shown in Figure 2, while iPSC-derived NKT cells in the switch culture showed mature $CD4^+$ or double-negative (DN) NKT cell phenotypes (Supplemental Figure 3B). These are similar to those obtained by the ESC culture as described (13). Therefore, Notch signaling inhibits phenotypic maturation of NKT cells.

The phenotypic maturation of iPSC-derived NKT cells with immature phenotypes occurs in vivo because the majority of iPSC-derived NKT cells, when transferred into $J\alpha18^{-/-}$ mice in vivo, developed downmodulated expression of CD24 and CD62L but augmented expression of CD44, CD69, CD122, and NKG2D (Supplemental Figure 8), similar to mature liver NKT cell phenotypes.

Most important is that, without maturation of cell surface phenotypes, iPSC-derived NKT cells acquire their potential to produce large amounts of IFN-γ, which is essential for in vivo adjuvant activity on antitumor responses. In fact, the iPSC-derived NKT cells obtained in the 25-day culture showed the ability to produce cytokines at levels similar to those of splenic NKT cells (Figure 2D and Figure 4G). In particular, IFN-γ production was significantly high in the 25-day culture system using OP9/Dll-1 (Figure 4G and Figure 2D), although, similar to ESC-derived NKT cells (13), iPSC-derived NKT cells mainly produced IL-4 but not IFN-γ in the 20-day culture system using OP9/Dll-1 (Supplemental Figure 3C). Therefore, IFN-γ production by iPSC-derived NKT cells is apparently due to the duration of the culture. In fact, iPSC-derived NKT cells produced large amounts of IFN-γ at culture day 25, but produced small amounts of IFN-γ at day 20 (see Figure 4G). Thus, immature cell surface phenotypes on iPSC-derived NKT cells generated in the present system do not correlate with their functional activity.

Taken collectively, the 25-day culture system using IL-7 and Flt3L and OP9/Dll-1 has several advantages; it yielded 10 times the number of NKT cells and produced 5 times the amount of IFN-γ (Figure 2D and Figure 4G) than what was obtained in the 20-day culture system (Supplemental Figure 3). Although the system we described here is a mouse model, it is helpful to establish methods for generation of iPSCs from human NKT cells and protocols for developing NKT cells from iPSCs suitable for clinical settings.

## Methods

*Cells.* The cells used in the present studies were ESCs (R1, E14); cloned ESCs, such as NKT-ES C-1 and NKT-ES D-1, obtained by direct nuclear transfer of B6 splenic NKT cells (13); MEFs (NKT-MEF) obtained from NKT B6 mice generated by the cloned ESCs; iPSCs (iPSC-7a, iPSC-7g) gen-

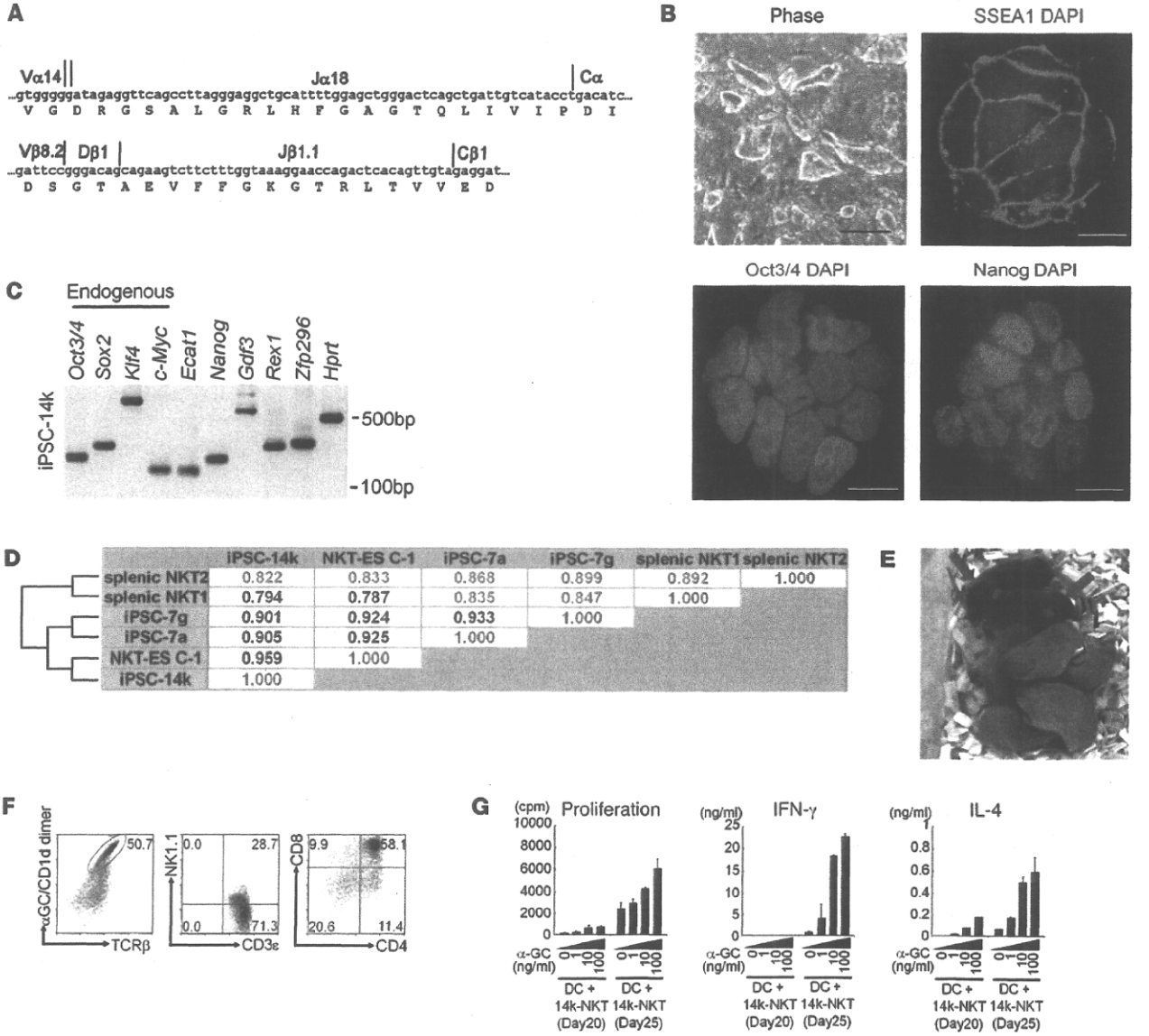


**Figure 4**

Generation of iPSC from splenic NKT cells and their development of iPSC-derived NKT cells with function in vitro. (**A**) Nucleotide and deduced amino acid sequences of the CDR3 junctional regions of the *Tcra* and *Tcrb* loci in iPSC-14k cells. (**B**) Colony shape and expression of SSEA1, Oct3/4, and Nanog in iPSC-14k. Scale bars: 100 μm (phase); 10 μm (immunofluorescence). (**C**) Expression of ESC marker genes in iPSC-14k cells analyzed by RT-PCR. (**D**) Analysis of global gene expression profiles comparing iPSC-14k cells to NKT-ES C-1, iPSC-7a, iPSC-7g, and splenic NKT cells. Note that the iPSC-14k cells are closely related to NKT-ES C-1, iPSC-7a, and iPSC-7g. (**E**) Offspring obtained by mating chimeras generated from the iPSC-14k cells and C57BL/6 females. Black coat color (indicated by arrows) represents germline transmission of iPSC-14k. (**F**) Expression of cell surface markers on the 14k-NKT cells. Numbers show percentage of each gate. (**G**) Proliferative response (left) and cytokine production (middle and right) by 14k-NKT cells (culture day 20 and day 25) upon stimulation with α-GalCer. Mean ± SD of triplicate wells is shown. One representative experiment of 3 is shown.

erated by NKT-MEF or iPSCs (iPSC-14k) by B6 splenic NKT cells; iPSC-derived NKT cells (7a-NKT, 7g-NKT, 14k-NKT); and splenic NKT cells.

*Generation of iPSCs.* NKT-MEF cells were reprogrammed by using retroviral vectors expressing *Oct3/4*, *Sox2*, *Klf4*, and *Nanog* according to the protocol established previously (14), which generated iPSC clones, such as iPSC-7a and iPSC-7g. The iPSCs from splenic NKT cell lines, such as iPSC-14k, were established by Yamanaka's method (14) using B6 splenic NKT cells ($1 \times 10^6$) activated with anti-CD3 and anti-CD28 in the presence of IL-12 and IL-2. Nucleotide sequences for primer pairs used for RT-PCR analysis of ESC markers are available in a previous report by Takahashi and Yamanaka (14). All animal studies were approved by the RIKEN Yokohama Institute Review Board.

*Genomic PCR.* Genomic DNA was isolated from cells using a Gentra Puregene kit (QIAGEN) for genotyping. Genomic PCR was performed with LA Taq (Takara). Primers used are listed in Supplemental Table 1.

*Immunofluorescence.* Immunofluorescence staining was performed using the following primary antibodies: anti–SSEA-1 (MAB4301; Milli-